Article

Cancer Cell

MUC1 and HIF-1alpha Signaling Crosstalk Induces Anabolic Glucose Metabolism to Impart Gemcitabine Resistance to Pancreatic Cancer

Graphical Abstract

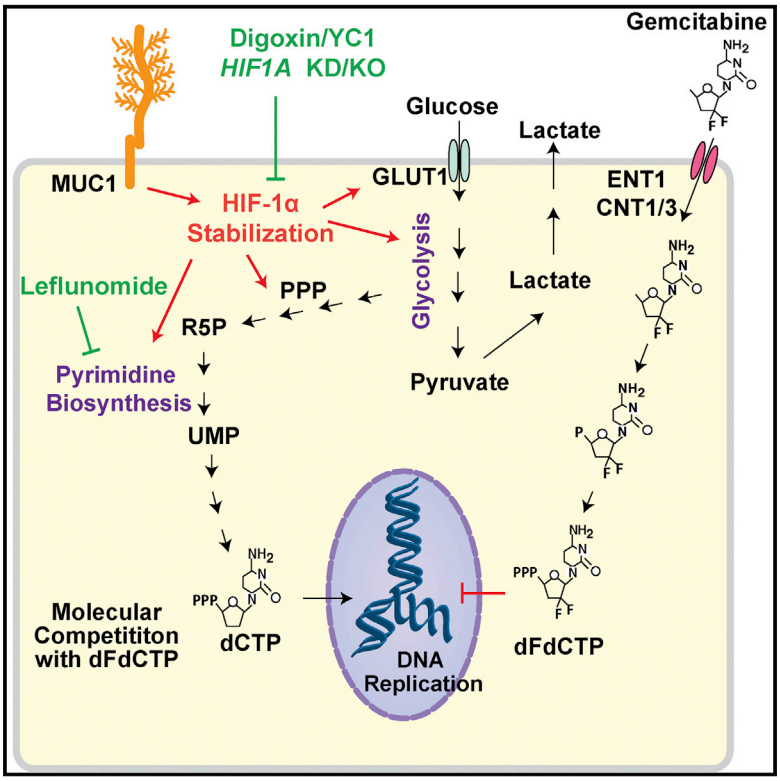

Highlights

- Gemcitabine resistance is associated with increased glucose uptake in PDAC
- HIF-1α upregulates non-oxidative PPP and pyrimidine biosynthesis
- HIF-1α is stabilized by MUC1 in gemcitabine-resistant tumors
- Targeting HIF-1α or metabolic pathways can sensitize PDAC tumors to gemcitabine

Authors

Surendra K. Shukla, Vinee Purohit, Kamiya Mehla, ..., Lewis C. Cantley, Lyudmyla Berim, Pankaj K. Singh

Correspondence

pankaj.singh@unmc.edu

In Brief

Shukla et al. identify that HIF-1α mediates increased glycolytic flux and *de novo* pyrimidine biosynthesis, leading to gemcitabine resistance in pancreatic cancer cells. Targeting HIF-1α or *de novo* pyrimidine biosynthesis increases the efficacy of gemcitabine.

Shukla et al., 2017, Cancer Cell *32*, 71–87
July 10, 2017
http://dx.doi.org/10.1016/j.ccell.2017.06.004

CellPress

Cancer Cell
Article

MUC1 and HIF-1alpha Signaling Crosstalk Induces Anabolic Glucose Metabolism to Impart Gemcitabine Resistance to Pancreatic Cancer

Surendra K. Shukla,[1,17] Vinee Purohit,[1,2,17] Kamiya Mehla,[1,17] Venugopal Gunda,[1] Nina V. Chaika,[1] Enza Vernucci,[1] Ryan J. King,[1] Jaime Abrego,[1] Gennifer D. Goode,[1] Aneesha Dasgupta,[1] Alysha L. Illies,[1] Teklab Gebregiworgis,[3] Bingbing Dai,[4] Jithesh J. Augustine,[4] Divya Murthy,[1] Kuldeep S. Attri,[1] Oksana Mashadova,[5] Paul M. Grandgenett,[1] Robert Powers,[3] Quan P. Ly,[6] Audrey J. Lazenby,[2] Jean L. Grem,[7] Fang Yu,[8] José M. Matés,[9] John M. Asara,[10] Jung-whan Kim,[11] Jordan H. Hankins,[12] Colin Weekes,[13] Michael A. Hollingsworth,[1] Natalie J. Sarkova,[14] Aaron R. Sasson,[15] Jason B. Fleming,[4] Jennifer M. Oliveto,[12] Costas A. Lyssiotis,[16] Lewis C. Cantley,[5] Lyudmyla Berim,[7] and Pankaj K. Singh[1,2,18,*]

[1]Eppley Institute for Research in Cancer and Allied Diseases, University of Nebraska Medical Center, Omaha, NE 68198-5950, USA
[2]Department of Pathology and Microbiology, University of Nebraska Medical Center, Omaha, NE 68198, USA
[3]Department of Chemistry, University of Nebraska-Lincoln, Lincoln, NE 68588, USA
[4]Department of Surgical Oncology, The University of Texas MD Anderson Cancer Center, Houston, TX 77030, USA
[5]Department of Medicine, Weill Cornell Medical College, New York, NY 10065, USA
[6]Department of Surgery, University of Nebraska Medical Center, Omaha, NE 68198, USA
[7]Department of Internal Medicine, University of Nebraska Medical Center, Omaha, NE 68198, USA
[8]Department of Biostatistics, University of Nebraska Medical Center, Omaha, NE 68198, USA
[9]Department of Molecular Biology and Biochemistry, University of Málaga and IBIMA, 29071 Málaga, Spain
[10]Department of Medicine, Harvard Medical School, Boston, MA 02115, USA
[11]Department of Biological Sciences, The University of Texas at Dallas, 800 West Campbell Road, Richardson, TX 75080, USA
[12]Department of Radiology, University of Nebraska Medical Center, Omaha, NE 68198, USA
[13]Division of Medical Oncology, University of Colorado School of Medicine, Aurora, CO 80045, USA
[14]Department of Anesthesiology, University of Colorado Denver, Aurora, CO 80045, USA
[15]Department of Surgery, Health Sciences Center T18-065, Stony Brook Medicine, Stony Brook, NY 11794, USA
[16]Department of Molecular and Integrative Physiology, University of Michigan, Ann Arbor, MI 48103, USA
[17]These authors contributed equally
[18]Lead Contact
*Correspondence: pankaj.singh@unmc.edu
http://dx.doi.org/10.1016/j.ccell.2017.06.004

SUMMARY

Poor response to cancer therapy due to resistance remains a clinical challenge. The present study establishes a widely prevalent mechanism of resistance to gemcitabine in pancreatic cancer, whereby increased glycolytic flux leads to glucose addiction in cancer cells and a corresponding increase in pyrimidine biosynthesis to enhance the intrinsic levels of deoxycytidine triphosphate (dCTP). Increased levels of dCTP diminish the effective levels of gemcitabine through molecular competition. We also demonstrate that MUC1-regulated stabilization of hypoxia inducible factor-1α (HIF-1α) mediates such metabolic reprogramming. Targeting HIF-1α or *de novo* pyrimidine biosynthesis, in combination with gemcitabine, strongly diminishes tumor burden. Finally, reduced expression of *TKT* and *CTPS*, which regulate flux into pyrimidine biosynthesis, correlates with better prognosis in pancreatic cancer patients on fluoropyrimidine analogs.

Significance

Multiple mechanisms have been proposed that lead to reduced effectiveness of gemcitabine in pancreatic cancer and yet resistance to gemcitabine still remains a challenge in the clinics. Aberrant metabolism is one of the important hallmarks of cancer that facilitates cancer cell survival and proliferation. The present study demonstrates existence of a widely prevalent metabolic mechanism that mediates chemotherapy resistance in pancreatic cancer. Utilizing cell-based models of acquired and intrinsic gemcitabine resistance, animal models, and patient-derived specimens, we identify key metabolic alterations that mediate gemcitabine resistance. Our studies provide potential targets to improve the efficacy of gemcitabine in patients.

INTRODUCTION

Poor response to therapies due to development of resistance in tumors remains a significant clinical challenge and contributes to overall poor patient prognosis. Gemcitabine, a deoxycytidine analog that inhibits DNA replication and thereby arrests tumor growth, is a widely used single-agent chemotherapy for pancreatic cancer (de Sousa Cavalcante and Monteiro, 2014). While still being utilized for the treatment of locally advanced or metastatic pancreatic cancer, the effectiveness of gemcitabine has been constrained by the frequent development of resistance to this drug in most of the treated patients (Heinemann et al., 2000). Recently, FOLFIRINOX (fluorouracil, leucovorin, irinotecan, and oxaliplatin) has been approved as a treatment for patients with advanced pancreatic ductal adenocarcinoma, showing significantly improved overall and median progression-free survival compared with gemcitabine, albeit, with a less favorable toxicity profile (Conroy et al., 2011). Furthermore, not all patients are equally responsive to FOLFIRINOX. Abraxane or albumin-bound paclitaxel along with gemcitabine is another combination therapy recently approved by the US Food and Drug Administration (Von Hoff et al., 2013). Gemcitabine, however, continues to be a part of this therapy. The efficacy of several anti-cancer therapies is linked to tumor cell survival and therefore to their effect on metabolic alterations in tumor cells (Fanciulli et al., 2000). Many previous studies have addressed only changes in the rate of influx or efflux of drug as a way of regulating the concentration of drug in the tumor cells for acquiring chemotherapy resistance. Hence, there is an urgent need to determine the metabolic mechanisms that hamper the efficiency of chemotherapy and to identify combinations that may significantly improve the efficacy of gemcitabine and other fluoropyrimidine analogs.

Large portions of solid tumors are hypoxic (Koong et al., 2000). Furthermore, most solid tumors, particularly pancreatic tumors, also demonstrate an increased accumulation of stromal tissue, i.e., desmoplasia. Increased desmoplasia and hypoxia have been implicated in the development of resistance to chemotherapy and radiotherapy (Yokoi and Fidler, 2004). Both desmoplasia and hypoxia also lead to the stabilization of hypoxia inducible factor-1α (HIF-1α), the master regulator of glucose metabolism (Semenza, 2010). Previous studies from our lab have demonstrated higher expression of HIF-1α and the corresponding downstream glucose metabolism genes in pancreatic tumor cells compared with the surrounding stroma (Chaika et al., 2012a, 2012b). Pancreatic cancers also metabolize glucose at higher rates (Dang, 2010; DeBerardinis et al., 2008; Vander Heiden et al., 2009). However, the precise fate of glucose and downstream metabolites and their role in therapy responsiveness is yet to be fully explored. Here, we delineate the metabolic alterations that facilitate gemcitabine resistance, utilizing pancreatic cancer as a model.

RESULTS

Increased Glucose Metabolism Fuels Gemcitabine Resistance in Gem-R Pancreatic Cancer Cells

To investigate the metabolic basis of gemcitabine resistance, we generated pancreatic cancer cell line (Capan-1, T3M4, and MIA PaCa-2) models with acquired gemcitabine resistance. For this, wild-type (WT) pancreatic cancer cells were cultured with increasing concentrations of gemcitabine over a period of approximately 6 months. The resistance status at each dose was determined by calculating the half maximal inhibitory concentration (IC_{50}) of gemcitabine using MTT cytotoxicity assays (Figure 1A). At the end of the 6-month treatment period, the cell lines generated (Gem-R) were approximately 500- to 1,000-fold more resistant compared with WT cells (Figure 1B). We observed an increase in clonogenic ability of the Capan-1 and T3M4 Gem-R cells under control and gemcitabine treatment, and increased colony number and size in soft agar assays (Figures S1A and S1B). To quantify the relative physiological glucose uptake by Gem-R cells compared with the WT cells, we performed [^{3}H]-2-deoxyglucose uptake assays after culturing the cells under normoxia (20% oxygen) or hypoxia (1% oxygen) for 12 hr. Capan-1 Gem-R, and T3M4 Gem-R cells displayed significantly increased glucose uptake in comparison with the controls, under normoxic as well as hypoxic conditions (Figure 1C). Similar alterations were observed for MIA PaCa-2 Gem-R cells (Figures S1C and S1D). Gem-R cells also demonstrated increased lactate release (Figures 1D and S1E). Expression of genes involved in glucose metabolism was also increased in Gem-R cells (Figure 1E).

To investigate the metabolic alterations underlying gemcitabine resistance, we performed liquid chromatography-coupled tandem mass spectrometry (LC-MS/MS)-based analysis (Gunda et al., 2016) followed by unsupervised hierarchical clustering. LC-MS/MS analysis indicated differential metabolite pools in Gem-R cells compared with WT controls (Figure 1F). Further analyses revealed an increase in the intermediate metabolites of glycolysis. Specifically, we observed an increase in metabolites upstream of dihydroxyacetone phosphate and glyceraldehyde-3-phosphate and increased intracellular pyruvate/lactate levels in Gem-R cells (Figure 1G).

To determine the dependence of the gemcitabine resistance phenotype on glucose metabolism, we cultured the Gem-R cells and the corresponding WT cells under low glucose conditions (0.5 mM glucose) for a short period (36 hr). Gem-R cells failed to respond to gemcitabine treatment but demonstrated significantly diminished survival under low glucose conditions (Figure 1H). Also, the intrinsically gemcitabine-resistant AsPC-1 and moderately resistant MIA PaCa-2 cells demonstrated significantly diminished cell survival under glucose-deprived conditions or under treatment with 2-DG (Figures S1F–S1I). Furthermore, in comparison with the WT cells, Gem-R cells demonstrated increased extracellular acidification rate (ECAR) and decreased oxygen consumption rate (OCR) (Figures 1I–1J and S1J). The partially gemcitabine-resistant cells demonstrated an intermediate increase in ECAR and decrease in OCR compared with the WT cells (Figures S1J–S1L). We sorted Capan-1 Gem-R cells for high and low glucose transporter 1 (GLUT1) expression. We observed an increased sensitivity to gemcitabine in Gem-R cells sorted for low surface GLUT1 expression (Figures 1K and S1M). However, we did not observe any significant difference in the sensitivity of WT and Gem-R cells against mitochondrial electron transport inhibitors such as metformin or oligomycin (Figure S1N). We also observed increased glucose uptake in tumors derived from

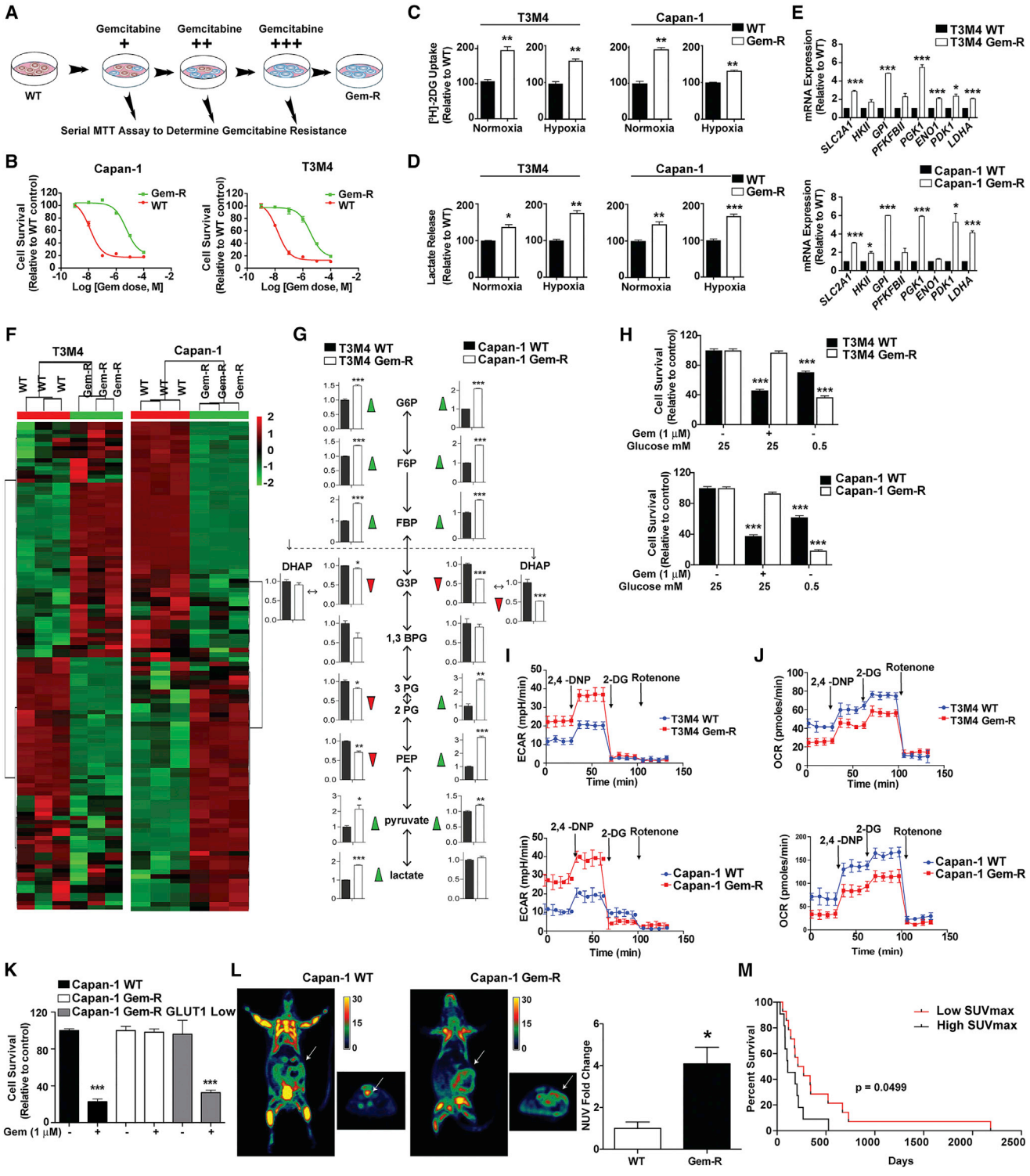

Figure 1. Increased Glucose Metabolism Fuels Gemcitabine Resistance in Gem-R Pancreatic Cells

(A) Acquired gemcitabine-resistant (Gem-R) Capan-1, and T3M4 pancreatic cancer cells were generated by exposing the corresponding wild-type (WT) cells to an increasing concentration of gemcitabine over 6 months. The resistance status was confirmed by performing MTT assays at each step. Red and blue colors of cells in the illustration denote sensitivity (or cell death) and resistance (or cell survival), respectively, based on response to gemcitabine treatment for 72 hr.

(B) Relative sensitivity of WT compared with the Gem-R pancreatic cancer cells as determined by MTT cytotoxicity assays. Cells were treated with increasing concentration of gemcitabine and MTT assays were performed 72 hr after treatment.

(legend continued on next page)

orthotopically implanted Gem-R cells in athymic nude mice, compared with that of the WT cells, by performing ^{18}F-fluorodeoxyglucose positron emission tomography (PET) imaging (Figure 1L). Furthermore, pancreatic cancer patients subjected to fluoropyrimidine analog-based therapies (gemcitabine or 5-fluorouracil [5-FU]) demonstrated a poor progression-free survival when high PET signal standardized uptake value (SUVmax $\geq$6) was observed in primary tumors (Figure 1M; Table S1,cohort 1). Together these findings establish that gemcitabine-resistant cells have an increased dependence on glucose metabolism.

Increased Glucose Carbon Flux through the Non-oxidative Pentose Phosphate Pathway in Gem-R Cells

LC-MS/MS-based metabolomics profiling of Gem-R cells revealed an increase in the steady-state levels of glucose metabolites through the non-oxidative arm of the pentose phosphate pathway (PPP) (Figures 2A and 2B). Moreover, we observed a significant reduction in the levels of oxidative PPP metabolites. Corroborating the metabolite levels, our qPCR findings demonstrated a significant increase in the expression of genes involved in the non-oxidative PPP in Gem-R cells and Gem-R cell-originated tumors (Figures 2C and S2A). Sedoheptulose-1,7-bisphosphate (SBP) was among the PPP metabolites increased in the Gem-R cells (Figure 2B), and it has been proposed that an increase in SBP indicates increased flux in the non-oxidative PPP (Ying et al., 2012). The gemcitabine IC_{50} value did not correlate with the expression levels of glucose-6-phosphate dehydrogenase (G6PD), a key gateway enzyme to the oxidative PPP, in 17 pancreatic cancer cell lines (Figure S2B). Likewise, we found no alteration in the activity of G6PD in Gem-R compared with WT cells (Figure S2C).

Steady-state levels are not always indicative of the flux of metabolites in a pathway, and hence we examined the relative contribution of non-oxidative versus oxidative PPP by performing 1-^{14}C- and 6-^{14}C-glucose labeling followed by measurement of $^{14}CO_2$ release. $^{14}CO_2$ from 1-^{14}C-glucose is released by both the oxidative PPP and the tricarboxylic acid (TCA) cycle, whereas $^{14}CO_2$ from 6-^{14}C-glucose can only be released via the TCA cycle. The release ratio of 1-^{14}C/6-^{14}C CO_2 was reduced in Gem-R cells compared with WT cells, indicating decreased flux of glucose through the oxidative PPP in Gem-R cells (Figure 2D). Furthermore, we examined the kinetics of U-^{13}C-glucose labeling of PPP metabolites in WT and Gem-R cells. We observed faster glucose flux into glycolytic metabolites, glucose-6-phosphate/fructose-6-phosphate and fructose-1,6-bisphosphate, in Gem-R cells, while slower kinetics were observed for oxidative PPP metabolite, 6-phosphogluconolactone (Figure 2E). We also observed faster and increased ^{13}C label incorporation in SBP, erythrose 4-phosphate, and phosphoribosyl pyrophosphate in Gem-R cells compared with WT cells. These results suggest increased glucose carbon flux through non-oxidative PPP in Gem-R cells.

Increased Pyrimidine Synthesis Contributes to Gemcitabine Resistance in Gem-R Cells

LC-MS/MS-based metabolomics followed by metabolic pathway and functional enrichment analysis demonstrated that the pyrimidine synthesis pathway is among the most significantly altered pathways in Gem-R cells compared with controls (Figure 3A). We performed oligonucleotide array analysis to determine the genes altered in Capan-1 Gem-R versus WT cells. We observed that Capan-1 Gem-R cells, compared with the WT cells, have increased expression of several genes involved in PPP and nucleotide biosynthesis pathways, including *TKT* (transketolase), *CTPS1* (cytidine triphosphate synthase), *TYMS* (thymidylate synthetase), *NME4* (NME/NM23 nucleoside diphosphate kinase 4), and *PRPSAP1* (phosphoribosyl pyrophosphate synthetase-associated protein 1) (Table S2). Correspondingly, we observed significant increases in N-carbamoyl-L-aspartate, dihydroorotate (DHOA), and uridine and cytidine metabolites (Figure 3B), all of which are metabolic intermediates in the pyrimidine synthesis pathway. We also performed qPCR to confirm the levels of genes involved in PPP and purine/pyrimidine nucleotide biosynthesis pathways in WT and Gem-R cells and tumors (Figures 3C and S3A). Combining the microarray data and the qPCR data in both cell lines, we observed a significant induction of *TKT* and *CTPS* (Figure 3C and Table S2), which would increase the flux of glucose carbon into the pyrimidine biosynthesis pathway. Previous studies have indicated that increased cytidine deaminase (CDA) levels may

(C) Relative glucose uptake in Gem-R and WT cells cultured under normoxia or hypoxia (1% oxygen). Counts for each group were normalized to the cell count in the respective group and plotted as a percent of WT control.
(D) Relative lactate release from Gem-R versus WT cells as determined by colorimetric analysis. Raw values were normalized to cell counts and plotted as percent of WT control.
(E) qPCR analysis for glycolytic genes in Gem-R cells relative to WT cells.
(F) Unsupervised hierarchical clustering of significantly deregulated metabolites between cells lines in Capan-1 WT and Gem-R cells.
(G) Major metabolites altered in the glycolytic pathway in Gem-R cells compared with the WT cells.
(H) Effect of glucose deprivation on the growth of WT and Gem-R cells. Cells were cultured in normal and low glucose (0.5 mM) conditions for 36 hr, with or without gemcitabine, followed by MTT assays. Relative survival is plotted as percent of WT or Gem-R cells cultured in normal glucose.
(I and J) WT and Gem-R cells were seeded in 24-well plates and exposed to 2,4-DNP, 2-DG, and rotenone to measure ECAR (I) and OCR (J).
(K) Relative gemcitabine sensitivity of Capan-1 Gem-R cells FACS sorted for low GLUT1 expression, compared with unsorted WT and Gem-R controls as determined by MTT assay values. Cell were treated with gemcitabine for 72 hr.
(L) Representative coronal (left) and axial (right) images of ^{18}F-fluorodeoxyglucose (FDG) uptake by positron emission tomography (PET) imaging in WT and Gem-R orthotopic implantation models (n = 6 mice per group). Normalized uptake values fold change for xenografts examined by FDG-PET are presented in the graph on the right. Uptake values were normalized with tumor volume.
(M) Kaplan-Meier progression-free survival analysis of pancreatic ductal adenocarcinoma (PDAC) patients on gemcitabine/5-FU chemotherapy with high (SUVmax $\geq$6; n = 11) or low (SUVmax <6; n = 14) [^{18}F]FDG-PET signal.
For all *in vitro* studies n = 3. Data are represented as mean ± SEM. The bar charts in (C, D, E, G, and L) were compared by Student's t test. Data in (H and K) were compared by one-way ANOVA followed by Tukey's *post hoc* test. Survival in (M) was compared by log rank (Mantel-Cox) test. *p < 0.05, **p < 0.01, and ***p < 0.001 compared with WT. See also Figure S1 and Table S1.

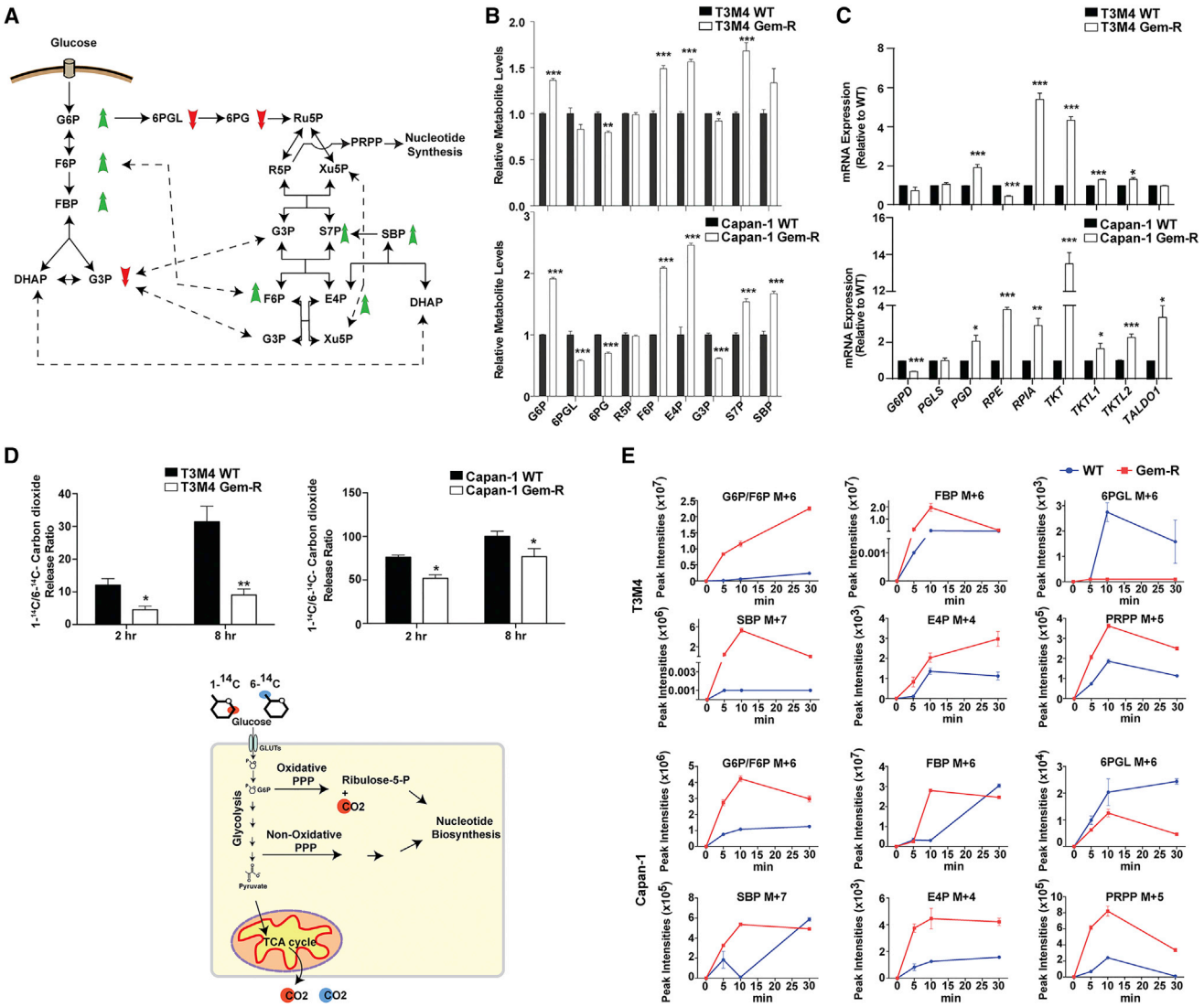

Figure 2. Increased Flux of Glucose Carbon through the Non-oxidative Pentose Phosphate Pathway in Gem-R Pancreatic Cells

(A) Summary of altered metabolites in Gem-R versus WT cells. An increase in metabolite levels is indicated with a green upward arrow and a reduction is indicated with a red downward arrow.

(B) The PPP metabolite levels in Gem-R relative to WT cells based on targeted LC-MS/MS metabolomics.

(C) Relative expression of the PPP genes in Gem-R versus WT cells determined by qPCR analysis.

(D) Radiolabeled CO_2 released from 1-^{14}C or 6-^{14}C glucose labeling in Gem-R versus WT cells. Raw scintillation counts were plotted as a ratio of 1-^{14}C/6-^{14}C-labeled carbon dioxide released at the indicated time points. Below is a schematic illustration of labeled carbon dioxide release generated from ^{14}C-labeled glucose at C1 or C6 positions.

(E) Kinetics of incorporation of ^{13}C label from U-^{13}C glucose into PPP metabolites in WT and Gem-R cells, as identified by LC-MS/MS analysis. M + X represents the number of ^{13}C-labeled carbon atoms in each metabolite, presented in arbitrary peak intensity units.

For all *in vitro* studies n = 3. Data are represented as mean ± SEM. The bar charts in (B and C) were compared by Student's t test. *p < 0.05, **p < 0.01, and ***p < 0.001. G6P, glucose 6-phosphate; F6P, fructose 6-phosphate; FBP, fructose 1,6-bisphosphate; DHAP, dihydroxyacetone phosphate; G3P, glyceraldehyde 3-phosphate; 6PGL, 6-Phosphogluconolactone; 6PG, 6-phosphogluconate; Ru5P, ribulose 5-phosphate; R5P, ribose 5-phosphate; Xu5P, xylulose 5-phosphate; PRPP, phosphoribosyl pyrophosphate; S7P, sedoheptulose 7-phosphate; SBP, sedoheptulose 1,7-bisphosphate; E4P, erythrose 4-phosphate. See also Figure S2.

also contribute to gemcitabine resistance (Weizman et al., 2014). However, we did not observe any significant difference in CDA mRNA levels in Gem-R cells compared with WT cells (Figure S3B).

Generation of orotate via dihydroorotate dehydrogenase (DHODH) is a crucial step in *de novo* pyrimidine biosynthesis. Therefore, in order to evaluate if the inhibition of DHODH itself could overcome gemcitabine resistance in pancreatic cancer, we treated the Gem-R and WT pancreatic cancer cell lines with 25 μM leflunomide, an inhibitor of DHODH (Ruckemann et al., 1998). Treatment with leflunomide significantly diminished orotate and downstream orotidine 5′-monophosphate levels,

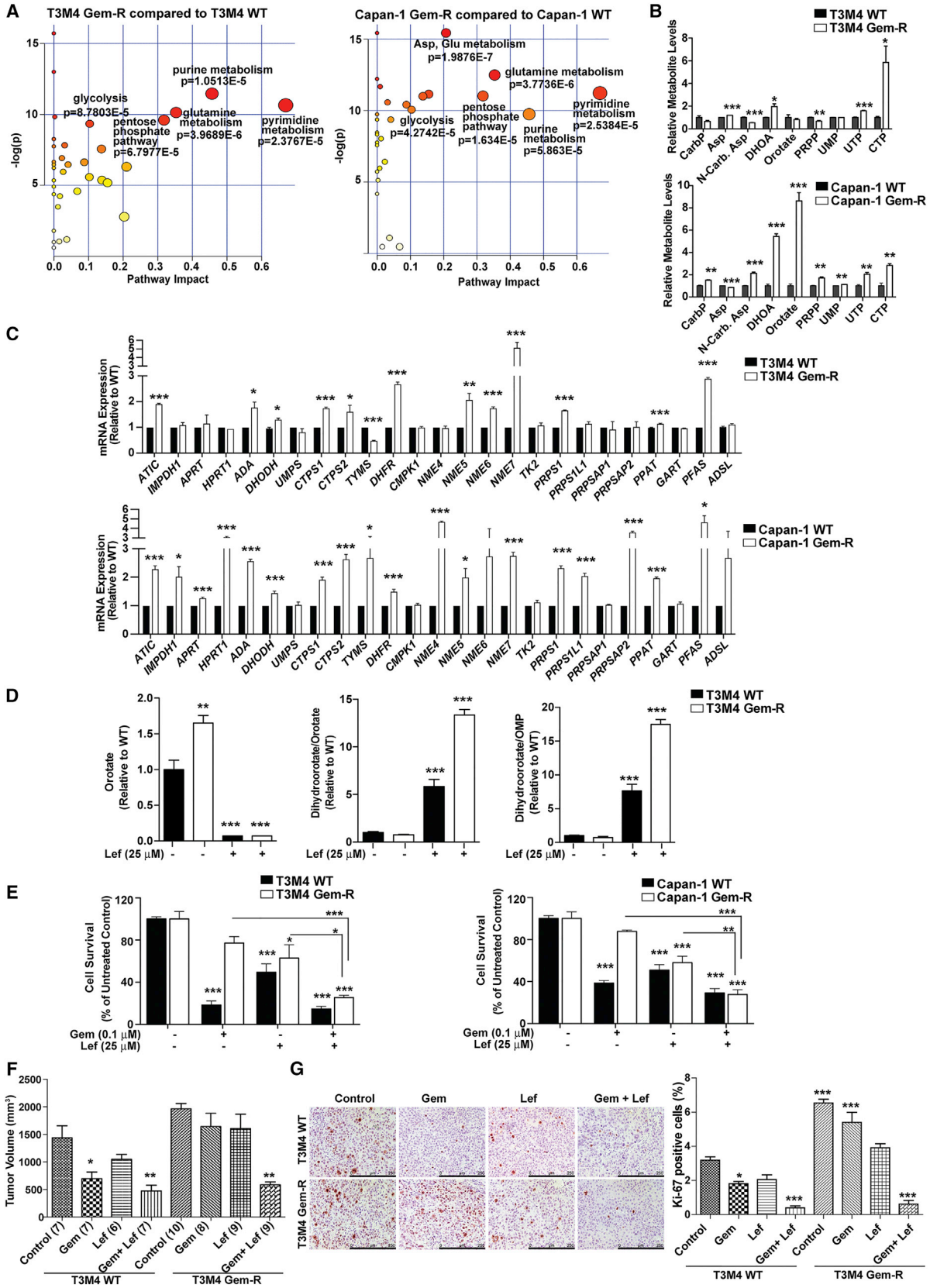

(legend on next page)

while causing an increase in the DHOA levels (Figure 3D), suggesting a blockade of DHODH activity. Leflunomide increased the efficacy of gemcitabine and inhibited cell survival in Capan-1 and T3M4 Gem-R cells (Figure 3E). In addition, there was a significant inhibition of cell survival in other pancreatic cancer cell lines when treated with both gemcitabine and leflunomide (Figure S3C). Furthermore, Gem-R cells showed a significant response to gemcitabine (50 mg/kg/day) in the presence of leflunomide (10 mg/kg/day) in orthotopic implantation models of pancreatic cancer, as observed by tumor volume, survival, and proliferation based on Ki-67 staining (Figures 3F–3G and S3D). However, we observed no noticeable body weight changes between different treatment groups (Figure S3E). These results indicate that Gem-R cells have increased pyrimidine biosynthesis and that their poor responsiveness to gemcitabine can be reversed at least in part by targeting pyrimidine biosynthesis.

Increased Deoxycytidine Reduces the Effectiveness of Gemcitabine in Gem-R Cells

Gemcitabine is a nucleoside analog, and hence both nucleoside synthesis and uptake direct its efficacy. Increased glycolysis in the Gem-R cells increases the flux of glycolytic intermediates through the non-oxidative PPP, causing an increase in the pyrimidine biosynthesis. ^{1}H-^{13}C heteronuclear single quantum coherence nuclear magnetic resonance analysis indicated an increase in all the nucleoside pools in Gem-R versus WT cells (Figures 4A and S4A). Increased synthesis of CTP might mitigate gemcitabine efficacy, so we investigated if increasing the cellular deoxycytidine levels could directly increase gemcitabine resistance in pancreatic cancer cells. We treated Capan-1 and T3M4 with 25 or 100 μM of deoxycytidine, and S2-013, SUIT-2, FG/Colo 357, and MIA PaCa-2 cells with 100 μM each of deoxycytidine, thymidine, deoxyguanosine, or deoxyadenosine, individually. Treatment with deoxycytidine, but not other nucleosides, increased resistance to gemcitabine in all of these cells (Figures 4B, 4C, S4B, and S4C). Resistance to gemcitabine might also occur due to reduced influx of gemcitabine into cancer cells. However, our data demonstrate that, even under untreated conditions, Gem-R cells have an increased expression of *SLC28A3* and *SLC29A1*, the principal nucleoside transporters involved in gemcitabine and deoxycytidine uptake (Figure S4D). Furthermore, we observed that, compared with the WT cells, Gem-R cells maintained a higher deoxycytidine pool and a lower gemcitabine/deoxycytidine ratio in the presence or absence of exogenous deoxycytidine (Figure 4D). We also observed that deoxycytidine nucleotide levels positively correlated with gemcitabine IC_{50} values in a panel of 15 pancreatic cancer cell lines (Figure 4E). In addition, we analyzed the deoxycytidine nucleotide pools in the flash-frozen tissue specimens from the Rapid Autopsy Program at the University of Nebraska Medical Center (UNMC) (Table S1, cohort 2). We observed significantly decreased progression-free survival with higher deoxycytidine or deoxyuridine, but not deoxyguanosine or deoxyadenosine, nucleotide pools in the primary tumors in patients who were subjected to gemcitabine or 5-FU (Figures 4F and S4E).

HIF-1α Is the Metabolic Master Regulator of Enhanced Glucose Metabolism and Pyrimidine Biosynthesis in Gemcitabine-Resistant Pancreatic Cancer Cells

HIF-1α is a key transcriptional regulator of glycolysis (Zhang et al., 2008). We observed that Gem-R cells express significantly higher levels of HIF-1α, even under normoxic conditions (Figures 5A and S4F). The Gem-R cells also demonstrate higher expression of HIF-1α-dependent enzymes, including GLUT1 and LDHA, which regulate glycolytic flux. The differences are further increased under hypoxic conditions. To determine if the increased glucose dependence of Gem-R cells is HIF dependent, we stably knocked down HIF-1α and HIF-2α in Capan-1 and T3M4 WT and Gem-R cells (Figure 5B). Knocking down HIF-1α inhibited glucose uptake in both WT and Gem-R pancreatic cancer cells (Figure 5C). Knocking down HIF-2α also decreased glucose uptake, but the effect was not as robust as for HIF-1α. Furthermore, knocking down HIF-1α diminished Gem-R cell survival under gemcitabine-treated conditions (Figure 5D). These findings indicate that, like WT cells, Gem-R cells depend on HIF-1α for enhanced uptake of glucose and that HIF-1α is required for gemcitabine resistance in these models.

Next, to determine if the role of HIF-1α in mediating gemcitabine resistance was exclusive to acquired resistant cells, we knocked down HIF-1α in intrinsically gemcitabine-resistant cells.

Figure 3. Gem-R Cells have Higher *De Novo* Pyrimidine Biosynthesis *In Vitro* and *In Vivo*

(A) Metabolic pathway impact analysis of significantly upregulated metabolites by Metaboanalyst 3.0 in Gem-R compared with WT cells.

(B) Levels of metabolites of *de novo* pyrimidine synthesis pathway in Gem-R cells relative to WT cells as determined by LC-MS/MS-based metabolomics.

(C) Relative mRNA expression levels of genes in the pyrimidine and the purine synthesis pathways analyzed by qPCR. Data analyzed by Student's t test and plotted relative to expression levels in WT cells.

(D) Levels of orotate and the ratios of dihydroorotate/orotate and dihydroorotate/orotidine 5′-monophosphate (OMP) in WT and Gem-R cells in the presence or absence of leflunomide relative to untreated WT cells. Data were analyzed by one-way ANOVA, followed by Bonferroni's *post hoc* test.

(E) Relative survival of Gem-R and WT cells by MTT assays, under treatment with gemcitabine, leflunomide, or gemcitabine with leflunomide. Data is presented relative to respective untreated shScr controls for WT and Gem-R cells. Comparisons made to the respective controls or indicated groups by two-way ANOVA, followed by Bonferroni's *post hoc* test.

(F) Tumor volumes upon necropsy, after 3 weeks of treatment, in orthotopically implanted mice subjected to treatments with control, gemcitabine (Gem), leflunomide (Lef), or gemcitabine with leflunomide (Gem + Lef). Numbers in parentheses indicate the number of mice in each cohort. All groups were compared with the control WT cohort by one-way ANOVA and Dunnett's *post hoc* test.

(G) IHC staining for Ki-67 and quantification of percent positive cells in the formalin-fixed tumor sections from the indicated treatment groups. Scale bars, 250 μm. Ki-67-positive and -negative cells were counted manually in ten fields of five tumors of each group. All groups were compared with the control WT cohort by one-way ANOVA and Tukey's *post hoc* test.

For all *in vitro* studies n = 3 per sample. Data are represented as mean ± SEM. *$p < 0.05$, **$p < 0.01$, and ***$p < 0.001$. CarP, carbamoyl phosphate; Asp, L-aspartate; N-Carb. Asp, N-carbamoyl-L-aspartate; DHOA, 4,5-dihydrooratate; PRPP, phosphoribosyl pyrophosphate; UMP, uridine 5′-monophosphate; UTP, uridine 5′-triphosphate; CTP, cytidine 5′-triphosphate. See also Figure S3 and Table S2.

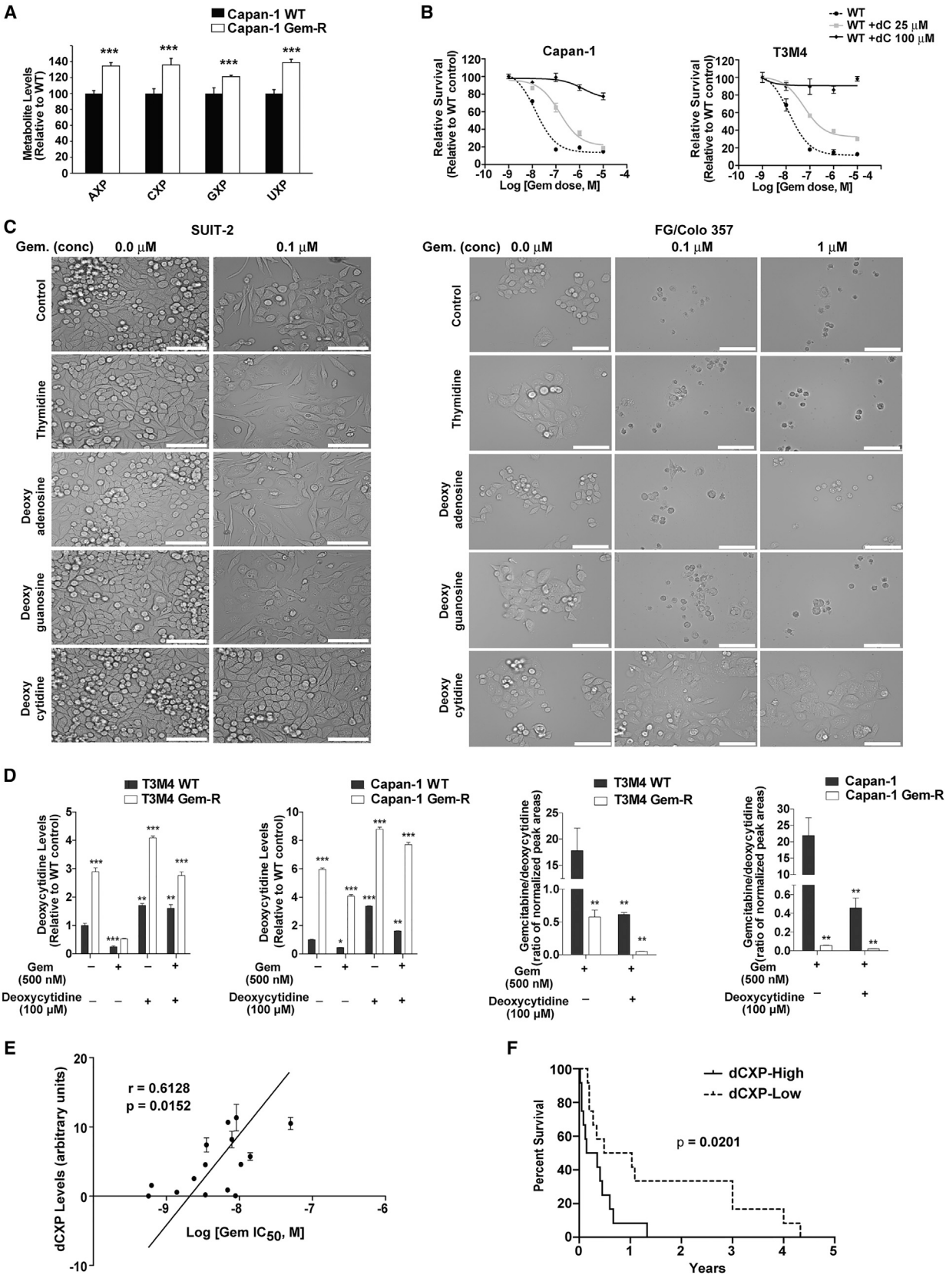

(legend on next page)

As observed in Gem-R cells, knocking down HIF-1α significantly diminished cell survival and glucose uptake in PANC-1 and, to a somewhat lesser extent, MIA PaCa-2 pancreatic cancer cell lines (Figures 5E–5G). We also observed a positive correlation between HIF-1α expression and gemcitabine IC_{50} in 15 pancreatic cancer cell lines (Figures S4G and S4H). In addition, we performed knockout of *HIF1A* by CRISPR/Cas9 in Gem-R cells and observed a similar increase in their responsiveness to gemcitabine (Figure 5H).

Next, we determined if the increased expression of *TKT* and *CTPS1* in Gem-R cells was regulated by HIF-1α. While regulation of *CTPS1* by HIF-1α is not known, *TKT* is a known HIF-1α target (Semenza, 2013; Zhao et al., 2010). We performed chromatin immunoprecipitation assays to determine HIF-1α occupancy on *TKT* and *CTPS1* gene promoters. We observed significantly increased occupancy of proximal and distal HIF-1α response elements (HRE) in the *CTPS1* promoter by HIF-1α in Gem-R cells compared with WT cells (Figure 5I). HIF-1α binding was further induced under hypoxic conditions and diminished by digoxin, a translational inhibitor of HIF-1α (Zhang et al., 2008). Similar trends were observed for HRE in the *TKT* promoter. In addition, we observed co-localization of TKT and CTPS with EF5, a hypoxia marker, and with CA IX, a marker of HIF-1α activity in orthotopically implanted Capan-1 cell-derived tumors (Figures 5J and 5K). We also observed a co-localization of TKT and CTPS with CA IX in human pancreatic ductal adenocarcinoma tissue sections (Figure 5L). These data indicate a role of HIF-1α in mediating resistance to gemcitabine by modulating the expression of *CTPS1, TKT,* and other glycolytic genes in pancreatic cancer cells.

Pharmacological Inhibition of HIF-1α Improves Gemcitabine Sensitivity

We next examined if HIF-1α inhibitor digoxin could abrogate gemcitabine resistance. Treatment with digoxin diminished HIF-1α levels in Capan-1 and T3M4 Gem-R cells (Figure 6A). Furthermore, digoxin reduced glucose uptake in Gem-R and WT cell lines (Figures S5A–S5C). Gem-R cells also demonstrated a significant reduction in the expression of genes involved in glucose metabolism under digoxin treatment (Figure S5D). Digoxin reduced deoxycytidine nucleotide levels and survival in response to gemcitabine in Gem-R cells (Figures 6B–6D). Altogether, these results provide evidence that HIF-1α promotes increased glucose dependence and gemcitabine resistance in pancreatic cancer cells.

Digoxin treatment reduces cell proliferation in breast and prostate cancer cell lines (Lin et al., 2009; Zhang et al., 2008, 2012), and it is currently in clinical trials for prostate cancer (Lin et al., 2014). To determine the efficacy of digoxin in gemcitabine-resistant pancreatic tumors, we orthotopically implanted WT or Gem-R cells in the pancreas of athymic nude mice. Starting at day 7 post-implantation, the mice were treated with digoxin, gemcitabine, or saline. Treatment with gemcitabine reduced tumor volume, glucose uptake, and proliferation in WT mice (Figures 6E–6K). However, we observed no significant reduction in tumor volume in the Gem-R tumor-bearing group due to gemcitabine treatment (Figures 6E and 6I). Digoxin treatment diminished tumoral glucose uptake and CA IX expression in mice in both groups (Figures 6F and 6G). A combination of gemcitabine and digoxin significantly diminished tumor volume and proliferation and increased survival in both WT and Gem-R groups (Figures 6E–6K and S5E). Treatment with YC1, another HIF-1α inhibitor, showed similar results (Figures 6I–6K). Treatment with combinations of digoxin or YC1 with gemcitabine also induced apoptosis (Figure 6J). Digoxin or YC1 did not cause any significant decrease in overall mouse body weight (Figures S5F and S5G). We also evaluated if genetic knockout of *HIF1A* would also sensitize tumor cells to gemcitabine. We observed a significant decrease in tumor burden, proliferative index, and CA IX staining upon treatment of *HIF1A* knockout WT or Gem-R cell-derived tumors with gemcitabine (Figures 6L–6O). We also evaluated the effect of gemcitabine and digoxin on patient-derived xenografts (PDXs) in athymic nude mice. Without affecting body weight, the combination of gemcitabine and digoxin significantly reduced growth, size, and proliferative index of tumors in mice (Figures 6P–6T and S5H). Taken together, these data indicate that targeting HIF-1α in combination with gemcitabine in Gem-R-tumor-bearing mice and PDX-implanted mice can abrogate tumor growth.

MUC1 Enhances HIF-1α Levels and Diminishes Gemcitabine Sensitivity in Gem-R Cells

We have previously demonstrated that MUC1, a large type 1 transmembrane protein, stabilizes and activates HIF-1α and increases glucose uptake and metabolism (Chaika et al., 2012a; Mehla and Singh, 2014). Our studies indicate that Gem-R cells have increased glucose and HIF-1α dependence. Interestingly, Gem-R cells also have increased MUC1 expression compared with the WT cells (Figure 7A). Hence, we further investigated if MUC1 expression is at least in part responsible for HIF-1α stabilization and the metabolic phenotype in our acquired gemcitabine resistance models. To achieve this, we generated Gem-R cells with stable knock down of *MUC1* (Figure 7B). *MUC1* knockdown Gem-R cells presented decreased

Figure 4. Increased Deoxycytidine Reduces the Efficacy of Gemcitabine

(A) NMR-based metabolite detection for nucleosides in Capan-1 Gem-R versus WT cells. X indicates the number of phosphate groups and can be mono-, di-, or triphosphates. Levels in Gem-R cells are presented relative to the WT control and analyzed by Student's t test.

(B) Effect of deoxycytidine (dC) on gemcitabine sensitivity in WT cells by MTT assays at 72 hr post-treatment.

(C) Bright-field images of SUIT-2 and FG/Colo 357 cells treated with gemcitabine and different nucleosides (100 μM) for 72 hr. Scale bars, 100 μm.

(D) Relative deoxycytidine levels and gemcitabine/deoxycytidine ratios as determined by LC-MS/MS in WT and Gem-R cells under treatment with gemcitabine and/or deoxycytidine. compared with untreated WT cells. Data were analyzed by one-way ANOVA and Bonferroni's *post hoc* test.

(E) Correlation of dCXP levels versus the IC_{50} of gemcitabine in 15 pancreatic cancer cell lines. "r" depicts Pearson correlation value and p values denote significance of correlation.

(F) Kaplan-Meier progression-free survival analysis of PDAC patients on gemcitabine/5-FU chemotherapy with high (above median; n = 12) or low (below median; n = 12) dCXP levels, as determined by LC-MS/MS in human pancreatic tumors. Data were compared with log rank (Mantel-Cox) test. For all *in vitro* studies n = 3 per sample. Data are represented as mean ± SEM. *$p < 0.05$, **$p < 0.01$, and ***$p < 0.001$ compared with WT controls. See also Figure S4 and Table S1.

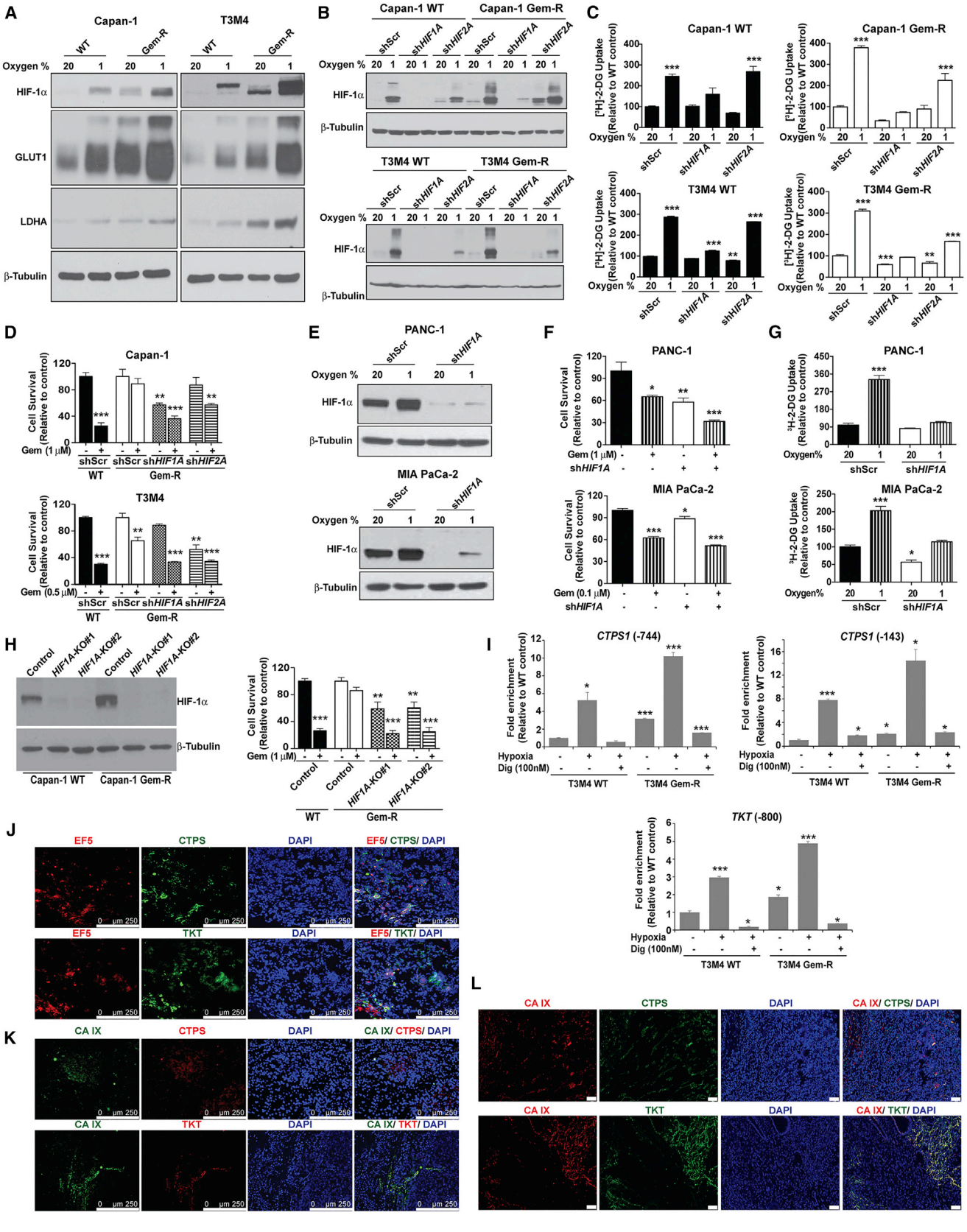

(legend on next page)

HIF-1α protein expression (Figure 7B) and reduced glucose uptake and lactate release (Figures 7C and 7D). Furthermore, knocking down *MUC1* significantly diminished gemcitabine resistance in Gem-R cells (Figure 7E).

Reduced CTPS and TKT Levels in Human Pancreatic Cancer Patients Correlate with Increased Gemcitabine Sensitivity

We investigated the levels of most genes involved in the PPP, pyrimidine, and purine synthesis pathways in 17 pancreatic cancer cell lines and correlated them with the IC_{50} of gemcitabine. We observed that gemcitabine resistance has a direct correlation with the expression of *TKT* and *CTPS* (Figure 8A). We also performed immunohistochemistry (IHC) studies on flash-frozen tissue sections from tumors from pancreatic cancer patients obtained through the Rapid Autopsy Program at the UNMC (Table S1, cohort 3). Our data revealed a significant increase in TKT and CTPS expression in primary and metastatic pancreatic cancer tissues compared with the normal pancreas (Figure 8B). Utilizing these patient data, we investigated if TKT/CTPS expression in primary tumors correlated with survival of patients treated with pyrimidine analog-based chemotherapy. Patients with higher CTPS or TKT expression in primary tumors had a significantly decreased progression-free survival (Figure 8C).

To summarize, gemcitabine-resistant tumors demonstrate increased HIF-1α-mediated glucose uptake. Glucose carbon is fed through both glycolysis and the non-oxidative PPP. Differentially increased carbon flux through the non-oxidative PPP and pyrimidine biosynthesis pathways leads to an increase in the cytoplasmic pools of deoxycytidine triphosphate (dCTP), which can outcompete gemcitabine from incorporating into the replicating DNA (Figure 8D). Inhibition of glycolysis or pyrimidine biosynthesis leads to increased gemcitabine sensitivity.

DISCUSSION

Drug resistance is the major cause of the failure of clinical effectiveness of chemotherapy. Pyrimidine analogs gemcitabine or 5-fluorouracil, alone or in combination with other drugs, are the current standard of care for advanced metastatic pancreatic cancer. However, the response to gemcitabine in patients is very poor with no drastic reduction in metastasis or increase in patient survival (Heinemann et al., 2000). Multiple molecular mechanisms of gemcitabine resistance encompassing different pathways have been suggested. However, most previous studies have mainly addressed acquired resistance due to changes in the rate of drug influx or efflux. Our current study presents strong evidence for the utility of agents targeting tumor cell metabolism in abrogating gemcitabine resistance in pancreatic cancer. Here, we present a mechanism of chemoresistance by which cancer cells increase intracellular cytidine pools that can in turn render gemcitabine ineffective by molecular competition.

Altered metabolism is one of the important hallmarks of cancer (Hanahan and Weinberg, 2011). The hypoxic microenvironment of pancreatic tumors stabilizes HIF-1α, which is the master regulator of glucose metabolism and induces glucose dependence in cancer cells (Semenza, 2003, 2009). The increased glucose uptake under hypoxia not only feeds into the glycolysis pathway, but also into intermediate pathways to generate biomass.

Figure 5. HIF-1α Regulates the Metabolic Phenotype and Gemcitabine Resistance in Pancreatic Cancer

(A) Expression of HIF-1α and HIF-1α-dependent gene products in WT versus Gem-R cells. Cells were cultured under normoxia (20% oxygen) or hypoxia (1% oxygen) for 12 hr, and the lysates were utilized for immunoblotting to determine the levels of HIF-1α, GLUT1, and LDHA. β-Tubulin was used as a loading control.

(B) WT and Gem-R cells were stably knocked down for *HIF1A* or *HIF2A* using shRNA. A scrambled shRNA (shScr) was used as a control. Knockdown status of HIF-1α was confirmed by immunoblotting lysates from cells cultured under normoxia and hypoxia for 6 hr, using β-tubulin as a loading control.

(C) Glucose uptake in WT and Gem-R cells as measured by [^{3}H]2DG labeling. Scrambled control (shScr), sh*HIF1A*, or sh*HIF2A* cells in each group were cultured under normoxia or hypoxia (1% oxygen) for 12 hr. Raw scintillation values were normalized to cell counts and depicted as percent of shScr WT/Gem-R controls.

(D) Gemcitabine responsiveness in shScr, sh*HIF1A*, or sh*HIF2A* Gem-R cells compared with the shScr WT cells. Cells were treated with gemcitabine for 72 hr, followed by MTT assays. Data are presented relative to respective untreated shScr controls for WT and Gem-R cells.

(E) PANC-1 and MIA PaCa-2 pancreatic cancer cells were assessed for knockdown of *HIF1A* by immunoblotting lysates from cells under normoxic and hypoxic conditions.

(F) Effect of *HIF1A*-knockdown on cell survival under gemcitabine-treated or untreated conditions for 72 hr as determined by MTT assays.

(G) Glucose uptake in shScr and sh*HIF1A* cells as measured by [^{3}H]2DG labeling. Cells in each group were cultured under normoxia or hypoxia (1% oxygen) for 12 hr. Raw scintillation values were normalized to cell counts and are plotted as percent of normoxic shScr cells.

(H) Evaluation of HIF-1α expression upon CRISPR/Cas9-mediated knockout of *HIF1A* (with two independent target regions of *HIF1A*, i.e., KO#1 and KO#2) in Capan-1 WT and Gem-R cells by western blotting (left). β-Tubulin was used as a loading control. Evaluation of the effect of *HIF1A* knockout on gemcitabine responsiveness by MTT assays in Capan-1 WT and Gem-R cells after 72 hr treatment (right). Data is presented relative to respective untreated controls for WT and Gem-R cells.

(I) Occupancy of *CTPS1* and *TKT* promoters by HIF-1α was assessed by ChIP using anti-HIF-1α Ab or IgG control, followed by qPCR analysis. Occupancy of HIF-1α at proximal (−143) and distal (−744) *CTPS1* promoter regions and *TKT* promoter region from T3M4 WT and T3M4 Gem-R cells under normoxic and hypoxic conditions (6 hr) is presented as relative to that in T3M4 WT cells under normoxic conditions.

(J) Co-localization of CTPS and TKT with 2-nitroimidazole (EF5; a hypoxia probe) in tumor sections from orthotopically implanted Capan-1 cells by immunofluorescence microscopy. Tumors were collected after 4 weeks of implantation. Scale bars, 250 μm.

(K) Co-localization of CTPS and TKT with CA IX in tumor sections from orthotopically implanted Capan-1 cells by immunofluorescence microscopy. Tumors were collected after 4 weeks of implantation. Scale bars, 250 μm.

(L) Co-localization of CTPS and TKT with CA IX in primary tumor sections from human pancreatic cancer patients. Scale bars, 50 μm.

For all *in vitro* studies n = 3 per sample. Data in bar charts were compared with the controls by one-way ANOVA with Tukey's *post hoc* analysis and are represented as mean ± SEM. *$p < 0.05$, **$p < 0.01$, and ***$p < 0.001$. See also Figure S4.

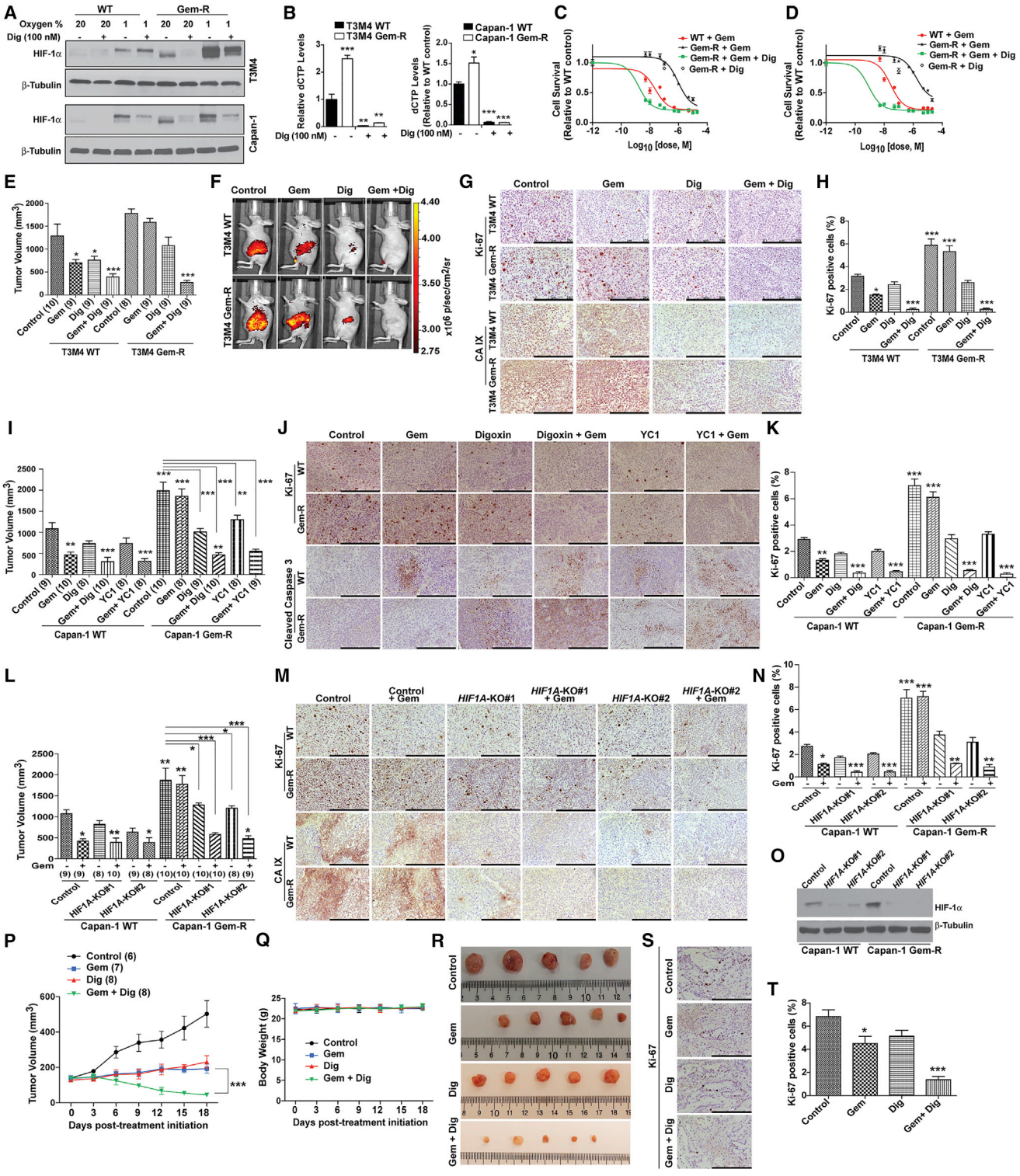

Figure 6. Pharmacological Inhibition of HIF-1α Improves Gemcitabine Sensitivity

(A) Immunoblotting for HIF-1α in T3M4 and Capan-1 WT and Gem-R cells cultured under normoxia or hypoxia (for 12 hr), treated with or without digoxin (Dig) for 12 hr.

(B) The dCTP levels relative to control WT cells, under treatment with solvent control or digoxin, as determined by LC-MS/MS. Values are presented relative to solvent control-treated WT cells.

(legend continued on next page)

Hypoxia has been linked with resistance in various cancers (Song et al., 2006), including pancreatic cancer (Yokoi and Fidler, 2004). A recent study by Lin et al. (2011) demonstrates that HIF-1α makes cells resistant to cisplatin, oxaliplatin, and paclitaxel. However, none of these studies directly determine the effect of HIF-1α or the underlying metabolic phenotype on gemcitabine sensitivity. Our data demonstrate that gemcitabine-resistant pancreatic cancer cells have increased expression of HIF-1α, accompanied by increased glycolytic phenotype and dependence on glucose. Previous studies from our lab indicate that the cytoplasmic tail of MUC1, a type I transmembrane protein, physically interacts with and prevents the proteasomal degradation of HIF-1α in pancreatic cancer cell lines and animal models (Chaika et al., 2012a) and, here, we observed increased expression of MUC1 in gemcitabine-resistant cells. Hence, we demonstrate that Gem-R cells stabilize HIF-1α by upregulating MUC1 expression. We also observed increased gemcitabine sensitization upon inhibition of HIF-1α in culture conditions, orthotopic implantation models, and PDX models.

Increased glycolysis serves to rapidly generate the biosynthetic intermediates to supply the ingredients for cell growth and proliferation. Our results indicate that increased glucose uptake in Gem-R cells is fed through the non-oxidative arm of PPP for *de novo* synthesis of pyrimidine nucleotides. *TKT* and *CTPS* are upregulated in Gem-R cells. Together, TKT and CTPS could serve to increase carbon flux into the pyrimidine biosynthetic pathway. Likewise, inhibition of DHODH, a key enzyme in the pyrimidine biosynthesis pathway, with leflunomide, increased gemcitabine sensitivity in the Gem-R cells. Previous studies show a TKT-mediated increase in the non-oxidative PPP in BCR-ABL-upregulated imatinib-resistant tumors (Zhao et al., 2010). It is possible that HIF-1α-mediated upregulation of TKT might be a common mechanism of survival in chemotherapy-resistant cancers. However, it is unlikely that pyrimidine synthesis would be essential for imatinib resistance in BCR-ABL tumors. Increased nucleotide synthesis in Gem-R cells leads to accumulation of dCTP and causes competitive inhibition of gemcitabine activity, thereby promoting gemcitabine resistance. While the Gem-R cells are able to take deoxycytidine and gemcitabine from extracellular milieu, they are able to maintain a higher deoxycytidine/gemcitabine ratio and hence sustain gemcitabine resistance. In addition, cell-extrinsic mechanisms of resistance have been identified, including drug scavenging by fibroblasts (Hessmann et al., 2017). The cell-intrinsic mechanisms of resistance identified in the current study are expected to operate in concert with the cell-extrinsic mechanisms of resistance.

For the last three decades gemcitabine has been the only single-agent treatment option for advanced metastatic pancreatic cancer patients (Burris and Storniolo, 1997). However, frequent development of resistance to this therapy contributes to poor prognosis of patients. Multiple molecular targets have been proposed to increase the efficacy of gemcitabine in pancreatic cancer; however, no significant advance has resulted so far from such efforts. Our study delineates the core metabolic alterations that mediate gemcitabine resistance in acquired as well as intrinsically resistant pancreatic cancer cells, thereby elucidating a widely prevalent metabolic mechanism of gemcitabine resistance. Targeting these core metabolic pathways could overcome gemcitabine resistance in pancreatic cancer.

STAR★METHODS

Detailed methods are provided in the online version of this paper and include the following:

- KEY RESOURCES TABLE
- CONTACT FOR REAGENT AND RESOURCE SHARING
- EXPERIMENTAL MODEL AND SUBJECT DETAILS
  - Cell Lines
  - Human Studies
- METHOD DETAILS
  - Glucose Uptake Assay
  - Mass Spectrometric Metabolomics Analysis

(C and D) Effect of digoxin treatment (100 nM) on gemcitabine responsiveness of T3M4 (C) and Capan-1 (D) Gem-R cells as determined by MTT assays, 72 hr after treatment with digoxin, a range of doses of gemcitabine, or both. Effect of digoxin alone on Gem-R cell survival, relative to DMSO-treated controls, is indicated by a single open diamond symbol.

(E–K) Effect of digoxin and YC1 on gemcitabine responsiveness in orthotopically implanted T3M4 (E–H) and Capan-1 (I–K) WT and Gem-R tumor models. Tumor volumes upon necropsy (after 3 weeks of treatment) in orthotopically implanted mice subjected to treatments with control, gemcitabine alone (50 mg/kg, biweekly), digoxin (2 mg/kg, daily), or YC1 (15 mg/kg, daily) alone, or gemcitabine with digoxin or YC1 (E and I). In vivo glucose uptake in tumor-bearing mice was determined 3 weeks after implantation; the mice were injected intraperitoneally with 100 μL of 10 nmol RediJect 2DG 750 probe and imaged 3 hr later (F). IHC staining for Ki-67 and CA IX or cleaved caspase-3 (G and J) and Ki-67 staining quantitation (H and K) in the formalin-fixed tumor sections from the indicated treatment groups.

(L–O) Effect of CRISPR/Cas9-mediated *HIF1A* knockout (with two independent target regions of *HIF1A*, i.e., KO#1 and KO#2) on gemcitabine responsiveness in orthotopically implanted Capan-1 WT and Gem-R tumor models. Tumor volumes upon necropsy, after 3 weeks of treatment, in orthotopically implanted mice subjected to treatments with control or gemcitabine (L). IHC staining for Ki-67 and CA IX (M) and Ki-67 staining quantitation (N) in the formalin-fixed tumor sections from the indicated treatment groups. Evaluation of *HIF1A* knockout status by western blotting in tumor extracts (O).

(P–T) Effect of digoxin on gemcitabine responsiveness in a patient-derived xenograft model. Tumor volumes measured by calipers at indicated time points in tumor-implanted mice subjected to treatments with control, gemcitabine alone (50 mg/kg, biweekly), digoxin (2 mg/kg, daily), or gemcitabine with digoxin. Tumor volumes were quantified by caliper measurements and statistically compared by two-way ANOVA analysis with Bonferroni's *post hoc* test; p value presented indicates comparison of tumor volumes in gemcitabine- and digoxin-treated mice at day 18 post-implantation with that of mice treated with gemcitabine alone (P). Body weights of mice with the indicated treatments (Q). Representative tumor images upon necropsy (R). IHC staining for Ki-67 (S) and Ki-67 staining quantitation (T). Ki-67-positive and -negative cells were counted manually in ten fields of five tumors of each group. Numbers in parentheses indicate the number of mice in each cohort.

For all *in vitro* studies n = 3 per sample. Data are represented as mean ± SEM. All cohorts in bar charts were compared with the respective controls by one-way ANOVA with Tukey's *post hoc* analysis. *$p < 0.05$, **$p < 0.01$, and ***$p < 0.001$. Scale bars, 250 μm. See also Figure S5.

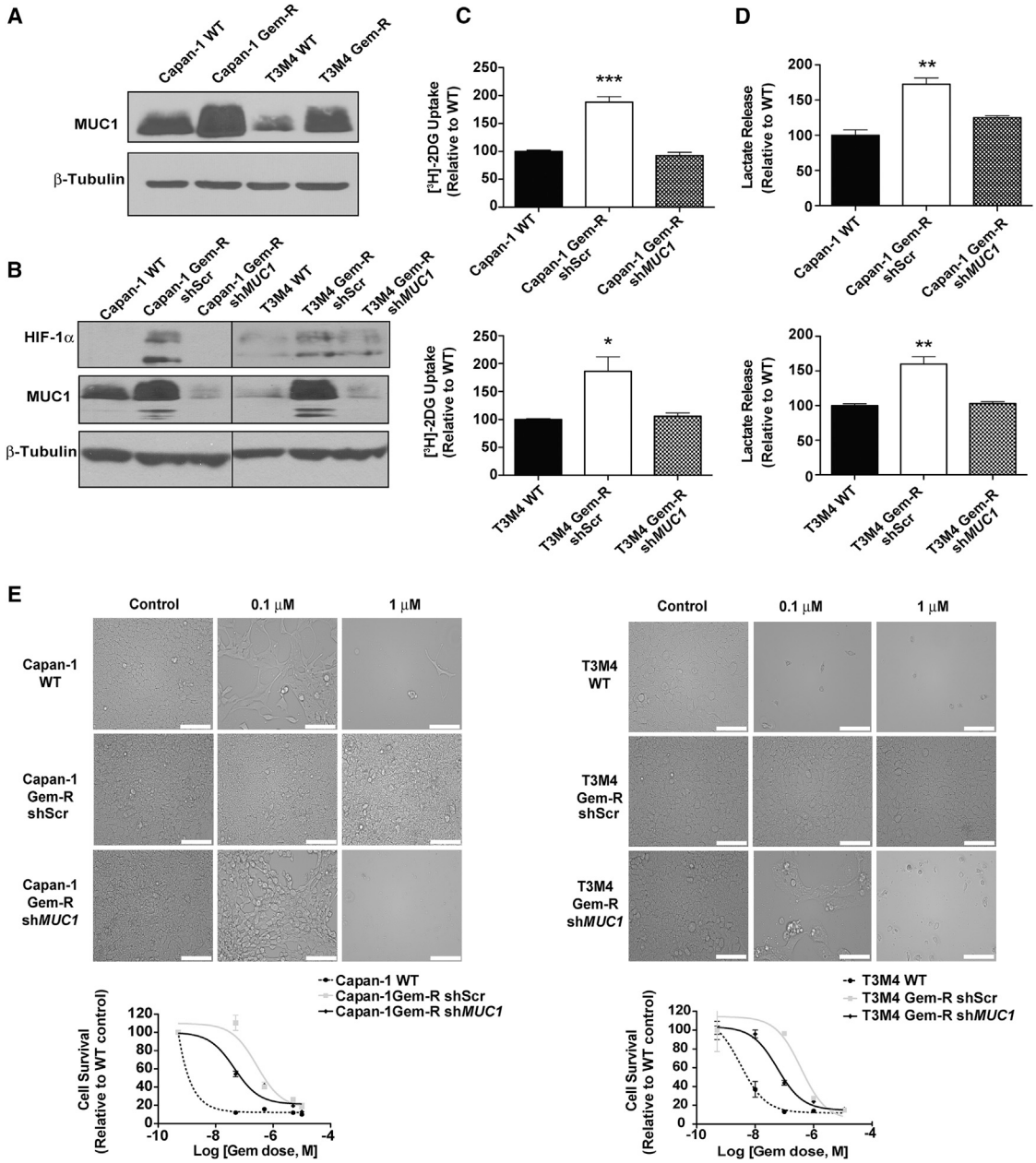

Figure 7. Knocking Down *MUC1* Abrogates HIF-1α Levels and Increases Gemcitabine Sensitivity in Gem-R Cells

(A) Relative MUC1 expression in Gem-R versus WT cells as determined by immunoblotting.

(B) MUC1 and HIF-1α protein levels in WT, Gem-R, and *MUC1* knockdown Gem-R cells, as determined by immunoblotting. β-Tubulin was used as a loading control.

(C) Relative glucose uptake determined by [^{3}H]2DG uptake assays in *MUC1* knockdown Gem-R compared with scrambled controls of Gem-R and WT cells. Raw scintillation values were normalized to cell counts and depicted as percent of shScr WT controls.

(D) Relative lactate release from shScr WT, shScr Gem-R, and *MUC1* knockdown Gem-R cells. Raw values were normalized to cell counts and plotted as percent of shScr WT controls.

(E) Effect of *MUC1* knockdown on gemcitabine sensitivity in Gem-R versus WT cells as denoted by pictomicrographs and survival curves. Scale bars, 100 μm. Cell survival was measured by MTT assay after 72 hr of gemcitabine treatment. Data in bar charts were compared by one-way ANOVA with Tukey's *post hoc* analysis.

For all *in vitro* studies n = 3 per sample. Data are represented as mean ± SEM. *$p < 0.05$, **$p < 0.01$, and ***$p < 0.001$.

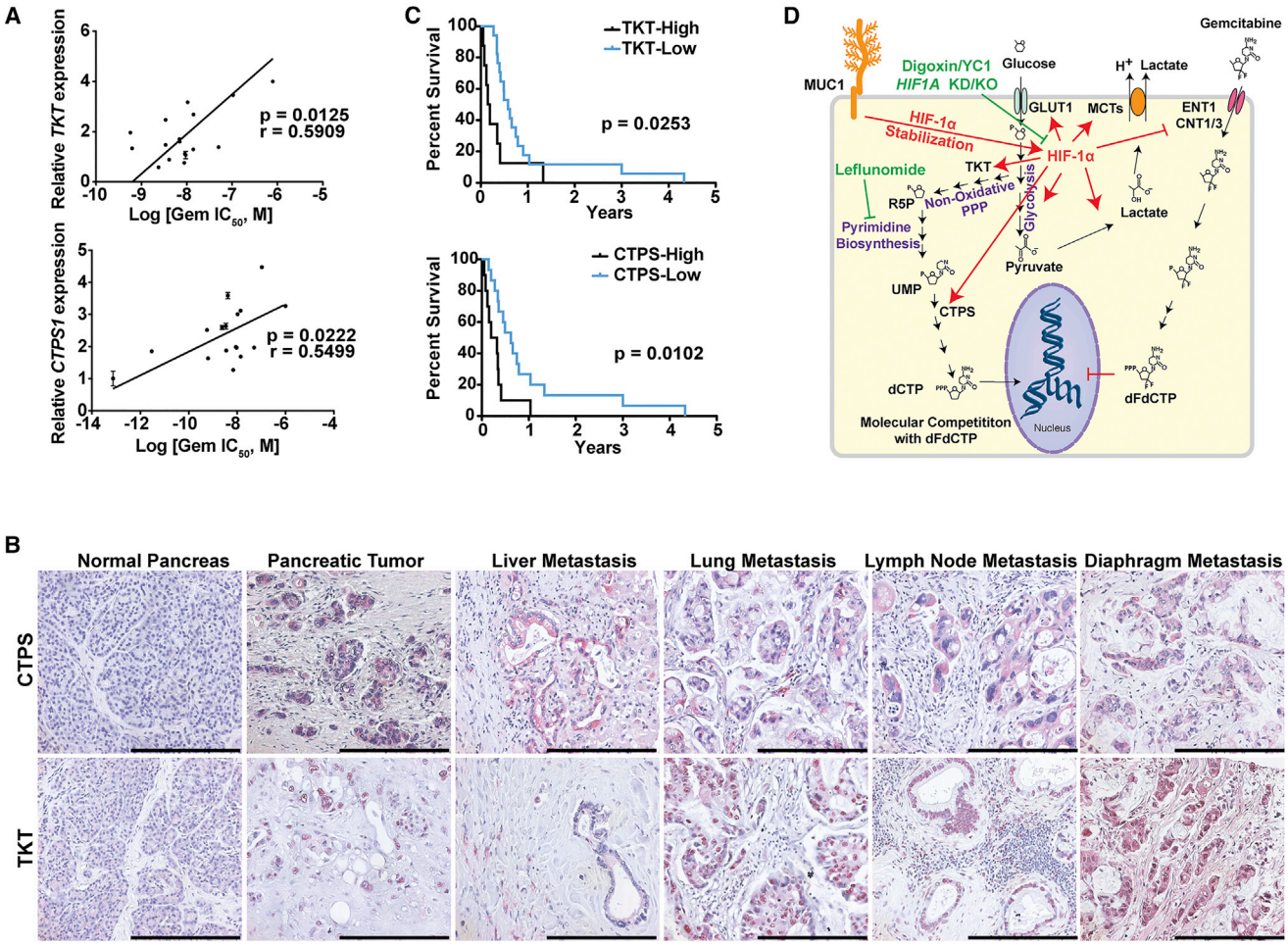

Figure 8. Reduced CTPS and TKT Levels Correlate with Increased Survival in Human Pancreatic Cancer Patients

(A) Correlation of *TKT* and *CTPS1* expression levels versus the IC_{50} of gemcitabine in 17 pancreatic cancer cell lines. "r" depicts Pearson correlation value, and p values denote significance of correlation.

(B) IHC staining of TKT and CTPS in formalin-fixed paraffin-embedded sections obtained from normal human pancreas, PDAC, and metastatic lesions. Scale bars, 250 μm.

(C) Kaplan-Meier progression-free survival analysis of PDAC patients on gemcitabine/5-FU chemotherapy with high (above a composite score of 9; n = 8 for TKT, n = 10 for CTPS) or low (below a composite score of 9; n = 17 for TKT, n = 15 for CTPS) TKT or CTPS expression levels based on IHC in pancreatic tumors. Comparisons were made by log rank (Mantel-Cox) test and p values denote significance of alterations in survival in TKT or CTPS high- versus low-expressing population.

(D) Graphical summary for the metabolic basis of gemcitabine resistance in pancreatic cancer. Gemcitabine-resistant cells demonstrate increased HIF-1α-mediated glucose uptake and, resultantly, increased flux of glucose through the PPP and pyrimidine biosynthesis to generate dCTP. Inhibition of HIF-1α or pyrimidine biosynthesis increases gemcitabine sensitivity in pancreatic cancer cells. R5P, ribose-5-phosphate; UMP, uridine 5′-monophosphate; dCTP, deoxycytidine 5′-triphosphate; dFdCTP, 2′,2′-difluorodeoxycytidine 5′-triphosphate or gemcitabine 5′-triphosphate. See also Table S1.

- Lentiviral Knockdown/Knockout
- FACS Sorting for GLUT1-High and -Low Cells
- MTT Cytotoxicity Assays
- Clonogenic Assays
- Soft Agar Assays
- Glutamine Uptake Assay
- XF24 Extracellular Flux Analysis
- 1-^{14}C- and 6-^{14}C-Glucose CO_2 Release Assay
- Lactate Release Assay
- Glucose-6-Phosphate Dehydrogenase Assay
- Gene Expression Analysis by Real-Time PCR (qPCR)
- Chromatin Immunoprecipitation Analysis
- Immunoblotting
- Immunohistochemistry
- Hypoxia Imaging and Co- localization with CTPS and TKT
- Tumor Growth Studies
- Patient-Derived Xenograft (PDX) Studies
- In Vivo Glucose Uptake Assays
- NMR Metabolite Extraction
- NMR Experiment
- NMR Data Analysis
- [^{18}F]FDG-PET, Magnetic Resonance Imaging
- Detection of Gemcitabine and dCTP

- LC-MS/MS for Polar Metabolites and ^{13}C-Glucose Based Flux Analysis
- QUANTIFICATION AND STATISTICAL ANALYSIS

SUPPLEMENTAL INFORMATION

Supplemental Information includes five figures and three tables and can be found with this article online at http://dx.doi.org/10.1016/j.ccell.2017.06.004.

AUTHOR CONTRIBUTIONS

S.K.S., V.P., K.M., V.G., N.J.S., J.B.F., C.A.L., L.B., and P.K.S. designed the research; S.K.S., V.P., K.M., V.G., N.V.C., E.V., R.J.K., J.A., G.D.G., A.D., A.L.I., T.G., B.D., J.J.A., D.M., K.S.A., O.M., J.M.A., N.J.S., and C.A.L. performed research; K.M., V.P., S.K.S., V.G., N.V.C., R.J.K., P.M.G., R.P., Q.P.L., J.L.G., J.M.M., J.-W.K., J.H.H., C.W., M.A.H., C.A.L., A.R.S., J.B.F., J.M.O., L.C.C., and P.K.S. contributed reagents/analytic tools; S.K.S., V.P., K.M., V.G., N.V.C., T.G., A.J.L., F.Y., J.B.F., J.M.O., C.A.L., L.B., and P.K.S. analyzed data; and S.K.S., V.P., K.M., V.G., N.J.S., J.B.F., C.A.L., and P.K.S. wrote the paper.

ACKNOWLEDGMENTS

We would like to thank Dr. Prakash Radhakrishnan for technical assistance with initial animal studies. This work was supported in part by funding from the NIH grants (R01 CA163649, R01 CA210439, and R01 CA216853, NCI) to P.K.S. and (P01CA117969) to L.C.C.; American Association for Cancer Research (AACR) – Pancreatic Cancer Action Network (PanCAN) Career Development Award (30-20-25-SING) to P.K.S.; the Specialized Programs for Research Excellence (SPORE, 2P50 CA127297, NCI) to P.K.S., J.L.G., and M.A.H.; Pancreatic Tumor Microenvironment Research Network (U54, CA163120, NCI) to P.K.S. and M.A.H.; and Lustgarten Foundation award to L.C.C. J.M.M. thanks SAF2015-64501-R. We would also like to acknowledge the Fred & Pamela Buffett Cancer Center Support Grant (P30CA036727, NCI) and NCCS COBRE (P30 GM106397, NIGMS) for supporting shared resources and the Animal Imaging Shared Resources of the University of Colorado Cancer Center (P30CA046934, NCI).

Received: June 13, 2016
Revised: March 1, 2017
Accepted: June 8, 2017
Published: July 10, 2017

REFERENCES

Akiyama, K., Chikayama, E., Yuasa, H., Shimada, Y., Tohge, T., Shinozaki, K., Hirai, M.Y., Sakurai, T., Kikuchi, J., and Saito, K. (2008). PRIMe: a Web site that assembles tools for metabolomics and transcriptomics. In Silico Biol. *8*, 339–345.

Behrens, M.E., Grandgenett, P.M., Bailey, J.M., Singh, P.K., Yi, C.H., Yu, F., and Hollingsworth, M.A. (2010). The reactive tumor microenvironment: MUC1 signaling directly reprograms transcription of CTGF. Oncogene *29*, 5667–5677.

Burris, H., and Storniolo, A.M. (1997). Assessing clinical benefit in the treatment of pancreas cancer: gemcitabine compared to 5-fluorouracil. Eur. J. Cancer *33* (*Suppl 1*), S18–S22.

Chaika, N.V., Gebregiworgis, T., Lewallen, M.E., Purohit, V., Radhakrishnan, P., Liu, X., Zhang, B., Mehla, K., Brown, R.B., Caffrey, T., et al. (2012a). MUC1 mucin stabilizes and activates hypoxia-inducible factor 1 alpha to regulate metabolism in pancreatic cancer. Proc. Natl. Acad. Sci. USA *109*, 13787–13792.

Chaika, N.V., Yu, F., Purohit, V., Mehla, K., Lazenby, A.J., DiMaio, D., Anderson, J.M., Yeh, J.J., Johnson, K.R., Hollingsworth, M.A., and Singh, P.K. (2012b). Differential expression of metabolic genes in tumor and stromal components of primary and metastatic loci in pancreatic adenocarcinoma. PLoS One *7*, e32996.

Cheng, T., Sudderth, J., Yang, C., Mullen, A.R., Jin, E.S., Mates, J.M., and DeBerardinis, R.J. (2011). Pyruvate carboxylase is required for glutamine-independent growth of tumor cells. Proc. Natl. Acad. Sci. USA *108*, 8674–8679.

Conroy, T., Desseigne, F., Ychou, M., Bouche, O., Guimbaud, R., Becouarn, Y., Adenis, A., Raoul, J.L., Gourgou-Bourgade, S., de la Fouchardiere, C., et al. (2011). FOLFIRINOX versus gemcitabine for metastatic pancreatic cancer. N. Engl. J. Med. *364*, 1817–1825.

Cui, Q., Lewis, I.A., Hegeman, A.D., Anderson, M.E., Li, J., Schulte, C.F., Westler, W.M., Eghbalnia, H.R., Sussman, M.R., and Markley, J.L. (2008). Metabolite identification via the Madison Metabolomics Consortium Database. Nat. Biotechnol. *26*, 162–164.

Dang, C.V. (2010). Rethinking the Warburg effect with Myc micromanaging glutamine metabolism. Cancer Res. *70*, 859–862.

De Meyer, T., Sinnaeve, D., Van Gasse, B., Tsiporkova, E., Rietzschel, E.R., De Buyzere, M.L., Gillebert, T.C., Bekaert, S., Martins, J.C., and Van Criekinge, W. (2008). NMR-based characterization of metabolic alterations in hypertension using an adaptive, intelligent binning algorithm. Anal. Chem. *80*, 3783–3790.

de Sousa Cavalcante, L., and Monteiro, G. (2014). Gemcitabine: metabolism and molecular mechanisms of action, sensitivity and chemoresistance in pancreatic cancer. Eur. J. Pharmacol. *741*, 8–16.

DeBerardinis, R.J., Lum, J.J., Hatzivassiliou, G., and Thompson, C.B. (2008). The biology of cancer: metabolic reprogramming fuels cell growth and proliferation. Cell Metab *7*, 11–20.

Fanciulli, M., Bruno, T., Giovannelli, A., Gentile, F.P., Di Padova, M., Rubiu, O., and Floridi, A. (2000). Energy metabolism of human LoVo colon carcinoma cells: correlation to drug resistance and influence of lonidamine. Clin. Cancer Res. *6*, 1590–1597.

Gunda, V., Yu, F., and Singh, P.K. (2016). Validation of metabolic alterations in microscale cell culture lysates using hydrophilic interaction liquid chromatography (HILIC)-tandem mass spectrometry-based metabolomics. PLoS One *11*, e0154416.

Hanahan, D., and Weinberg, R.A. (2011). Hallmarks of cancer: the next generation. Cell *144*, 646–674.

Heinemann, V., Wilke, H., Mergenthaler, H.G., Clemens, M., Konig, H., Illiger, H.J., Arning, M., Schalhorn, A., Possinger, K., and Fink, U. (2000). Gemcitabine and cisplatin in the treatment of advanced or metastatic pancreatic cancer. Ann. Oncol. *11*, 1399–1403.

Hessmann, E., Patzak, M.S., Klein, L., Chen, N., Kari, V., Ramu, I., Bapiro, T.E., Frese, K.K., Gopinathan, A., Richards, F.M., et al. (2017). Fibroblast drug scavenging increases intratumoural gemcitabine accumulation in murine pancreas cancer. Gut. http://dx.doi.org/10.1136/gutjnl-2016-311954.

Kim, M.P., Evans, D.B., Wang, H., Abbruzzese, J.L., Fleming, J.B., and Gallick, G.E. (2009). Generation of orthotopic and heterotopic human pancreatic cancer xenografts in immunodeficient mice. Nat. Protoc. *4*, 1670–1680.

Koong, A.C., Mehta, V.K., Le, Q.T., Fisher, G.A., Terris, D.J., Brown, J.M., Bastidas, A.J., and Vierra, M. (2000). Pancreatic tumors show high levels of hypoxia. Int. J. Radiat. Oncol. Biol. Phys. *48*, 919–922.

Lin, J., Denmeade, S., and Carducci, M.A. (2009). HIF-1alpha and calcium signaling as targets for treatment of prostate cancer by cardiac glycosides. Curr. Cancer Drug Targets *9*, 881–887.

Lin, S.C., Chien, C.W., Lee, J.C., Yeh, Y.C., Hsu, K.F., Lai, Y.Y., Lin, S.C., and Tsai, S.J. (2011). Suppression of dual-specificity phosphatase-2 by hypoxia increases chemoresistance and malignancy in human cancer cells. J. Clin. Invest. *121*, 1905–1916.

Lin, J., Zhan, T., Duffy, D., Hoffman-Censits, J., Kilpatrick, D., Trabulsi, E.J., Lallas, C.D., Chervoneva, I., Limentani, K., Kennedy, B., et al. (2014). A pilot phase II study of digoxin in patients with recurrent prostate cancer as evident by a rising PSA. Am. J. Cancer Ther. Pharmacol. *2*, 21–32.

Mehla, K., and Singh, P.K. (2014). MUC1: a novel metabolic master regulator. Biochim. Biophys. Acta *1845*, 126–135.

Morelli, M.P., Tentler, J.J., Kulikowski, G.N., Tan, A.C., Bradshaw-Pierce, E.L., Pitts, T.M., Brown, A.M., Nallapareddy, S., Arcaroli, J.J., Serkova, N.J., et al. (2012). Preclinical activity of the rational combination of selumetinib

(AZD6244) in combination with vorinostat in KRAS-mutant colorectal cancer models. Clin. Cancer Res. *18*, 1051–1062.

Nguyen, B.D., Meng, X., Donovan, K.J., and Shaka, A.J. (2007). SOGGY: solvent-optimized double gradient spectroscopy for water suppression. A comparison with some existing techniques. J. Magn. Reson. *184*, 263–274.

Ruckemann, K., Fairbanks, L.D., Carrey, E.A., Hawrylowicz, C.M., Richards, D.F., Kirschbaum, B., and Simmonds, H.A. (1998). Leflunomide inhibits pyrimidine de novo synthesis in mitogen-stimulated T-lymphocytes from healthy humans. J. Biol. Chem. *273*, 21682–21691.

Schlaepfer, I.R., Glode, L.M., Hitz, C.A., Pac, C.T., Boyle, K.E., Maroni, P., Deep, G., Agarwal, R., Lucia, S.M., Cramer, S.D., et al. (2015). Inhibition of lipid oxidation increases glucose metabolism and enhances 2-deoxy-2-[(18)F] fluoro-D-glucose uptake in prostate cancer mouse xenografts. Mol. Imaging Biol. *17*, 529–538.

Schmittgen, T.D., and Livak, K.J. (2008). Analyzing real-time PCR data by the comparative C(T) method. Nat. Protoc. *3*, 1101–1108.

Semenza, G.L. (2003). Targeting HIF-1 for cancer therapy. Nat. Rev. Cancer *3*, 721–732.

Semenza, G.L. (2009). Regulation of oxygen homeostasis by hypoxia-inducible factor 1. Physiology *24*, 97–106.

Semenza, G.L. (2010). Defining the role of hypoxia-inducible factor 1 in cancer biology and therapeutics. Oncogene *29*, 625–634.

Semenza, G.L. (2013). HIF-1 mediates metabolic responses to intratumoral hypoxia and oncogenic mutations. J. Clin. Invest. *123*, 3664–3671.

Shukla, S.K., Gebregiworgis, T., Purohit, V., Chaika, N.V., Gunda, V., Radhakrishnan, P., Mehla, K., Pipinos, I.I., Powers, R., Yu, F., and Singh, P.K. (2014). Metabolic reprogramming induced by ketone bodies diminishes pancreatic cancer cachexia. Cancer Metab. *2*, 18.

Singh, P.K., Behrens, M.E., Eggers, J.P., Cerny, R.L., Bailey, J.M., Shanmugam, K., Gendler, S.J., Bennett, E.P., and Hollingsworth, M.A. (2008). Phosphorylation of MUC1 by Met modulates interaction with p53 and MMP1 expression. J. Biol. Chem. *283*, 26985–26995.

Song, X., Liu, X., Chi, W., Liu, Y., Wei, L., Wang, X., and Yu, J. (2006). Hypoxia-induced resistance to cisplatin and doxorubicin in non-small cell lung cancer is inhibited by silencing of HIF-1alpha gene. Cancer Chemother. Pharmacol. *58*, 776–784.

Vander Heiden, M.G., Cantley, L.C., and Thompson, C.B. (2009). Understanding the Warburg effect: the metabolic requirements of cell proliferation. Science *324*, 1029–1033.

Von Hoff, D.D., Ervin, T., Arena, F.P., Chiorean, E.G., Infante, J., Moore, M., Seay, T., Tjulandin, S.A., Ma, W.W., Saleh, M.N., et al. (2013). Increased survival in pancreatic cancer with nab-paclitaxel plus gemcitabine. N. Engl. J. Med. *369*, 1691–1703.

Weizman, N., Krelin, Y., Shabtay-Orbach, A., Amit, M., Binenbaum, Y., Wong, R.J., and Gil, Z. (2014). Macrophages mediate gemcitabine resistance of pancreatic adenocarcinoma by upregulating cytidine deaminase. Oncogene *33*, 3812–3819.

Wishart, D.S., Jewison, T., Guo, A.C., Wilson, M., Knox, C., Liu, Y., Djoumbou, Y., Mandal, R., Aziat, F., Dong, E., et al. (2013). HMDB 3.0 – the human metabolome database in 2013. Nucleic Acids Res. *41*, D801–D807.

Worley, B., and Powers, R. (2014). MVAPACK: a complete data handling package for NMR metabolomics. ACS Chem. Biol. *9*, 1138–1144.

Wu, M., Neilson, A., Swift, A.L., Moran, R., Tamagnine, J., Parslow, D., Armistead, S., Lemire, K., Orrell, J., Teich, J., et al. (2007). Multiparameter metabolic analysis reveals a close link between attenuated mitochondrial bioenergetic function and enhanced glycolysis dependency in human tumor cells. Am. J. Physiol. Cell Physiol. *292*, C125–C136.

Xia, J., and Wishart, D.S. (2016). Using MetaboAnalyst 3.0 for comprehensive metabolomics data analysis. Curr. Protoc. Bioinformatics *55*, 14.10.1–14.10.91.

Ying, H., Kimmelman, A.C., Lyssiotis, C.A., Hua, S., Chu, G.C., Fletcher-Sananikone, E., Locasale, J.W., Son, J., Zhang, H., Coloff, J.L., et al. (2012). Oncogenic Kras maintains pancreatic tumors through regulation of anabolic glucose metabolism. Cell *149*, 656–670.

Yokoi, K., and Fidler, I.J. (2004). Hypoxia increases resistance of human pancreatic cancer cells to apoptosis induced by gemcitabine. Clin. Cancer Res. *10*, 2299–2306.

Yuan, M., Breitkopf, S.B., Yang, X., and Asara, J.M. (2012). A positive/negative ion-switching, targeted mass spectrometry-based metabolomics platform for bodily fluids, cells, and fresh and fixed tissue. Nat. Protoc. *7*, 872–881.

Zhang, H., Qian, D.Z., Tan, Y.S., Lee, K., Gao, P., Ren, Y.R., Rey, S., Hammers, H., Chang, D., Pili, R., et al. (2008). Digoxin and other cardiac glycosides inhibit HIF-1alpha synthesis and block tumor growth. Proc. Natl. Acad. Sci. USA *105*, 19579–19586.

Zhang, H., Wong, C.C., Wei, H., Gilkes, D.M., Korangath, P., Chaturvedi, P., Schito, L., Chen, J., Krishnamachary, B., Winnard, P.T., Jr., et al. (2012). HIF-1-dependent expression of angiopoietin-like 4 and L1CAM mediates vascular metastasis of hypoxic breast cancer cells to the lungs. Oncogene *31*, 1757–1770.

Zhao, F., Mancuso, A., Bui, T.V., Tong, X., Gruber, J.J., Swider, C.R., Sanchez, P.V., Lum, J.J., Sayed, N., Melo, J.V., et al. (2010). Imatinib resistance associated with BCR-ABL upregulation is dependent on HIF-1alpha-induced metabolic reprograming. Oncogene *29*, 2962–2972.

STAR★METHODS

KEY RESOURCES TABLE

REAGENT	SOURCE	IDENTIFIER
Antibodies		
Purified Mouse Anti-Human HIF1-α	BD Biosciences	Cat# 610959; RRID:AB_610959
Anti-MUC1 antibody[CT2]	Abcam	Cat# ab80952; RRID:AB_1640314
Anti-Glucose Transporter GLUT1 antibody	Abcam	Cat# ab 15309; RRID:AB_301844
LDHA(C4B5) Rabbit mAb	Cell Signaling Technology	Cat# 3582; RRID:AB_2066887
Cleaved Caspase-3 (Asp175) Antibody	Cell Signaling Technology	Cat# 9661; RRID:AB_2341188
Ki-67, Rabbit Monoclonal Antibody	Thermo Fischer Scientific	Cat# RM9106-SO; RRID:AB_2341197
Anti-CTPS (416-430) antibody produced in rabbit	Sigma-Aldrich	Cat# SAB1101071; RRID:AB_10606733
Anti-TKT antibody produced in rabbit	Sigma-Aldrich	Cat# HPA029481; RRID:AB_10558885
Human Carbonic Anhydrase IX/CA9 Antibody	Thermo Fischer Scientific	Cat# MA5-16318; RRID:AB_2537837
Beta-tubulin (E7)	Developmental Studies Hybridoma Bank, University of Iowa	Cat#AB2315513; RRID:AB_528499
Cy3-conjugated anti-EF5antibody	Gift from Prof. Cameron J Koch	N/A
Chemicals		
2-Deoxy-D-glucose	Sigma-Aldrich	Cat# D8375
[^{3}H] 2-Deoxy-D-glucose	Perkin Elmer	Cat# NET328A001MC
RediJect 2-DG Fluorescent Imaging Probe	Perkin Elmer	Cat#760561
Gemcitabine	Teva Parenteral Medicine Inc	Cat#NDC0703-5778-01
YC1	Tocris Bioscience	Cat# 4307/50
Digoxin	Sigma-Aldrich	Cat# D6770
3-(4,5-Dimethyl-2-thiazolyl)-2,5-diphenyl-2H-tetrazolium bromide (MTT)	Sigma-Aldrich	Cat# M2128
2′-Deoxycytidine	Sigma-Aldrich	Cat# D3897
2′-Deoxyadenosine monohydrate	Sigma-Aldrich	Cat# D8668
2′-Deoxyguanosinemonohydrate	Sigma-Aldrich	Cat# 854999
Thymidine	Sigma-Aldrich	Cat# T1895
Acivicin	Sigma-Aldrich	Cat# SML0312
Leflunomide	Enzo Life Sciences	Cat# ALX-430-093-M050
Digoxin (500 mcg/2ml)	West-Ward Pharmaceuticals, NJ	Cat# 0641-1410-35
D-GLUCOSE (U-13C6, 99%)	Cambridge Isotope Laboratories, Inc.	Cat# CLM-1396-PK
Glucose, D[1-^{14}C]	Perkin Elmer	Cat# NEC043X001MC
Glucose, D[^{14}C(U)]	Perkin Elmer	Cat# NEC042X001MC
Glucose, D[6-^{14}C]	Perkin Elmer	Cat# NEC045X050MC
Rotenone	Sigma-Aldrich	Cat# R8875
2,4-Dinitrophenol	Sigma-Aldrich	Cat# D198501
EF5	Gift from Prof. Cameron J Koch	N/A
Critical Commercial Assays		
L-Lactate Assay Kit	Eton Bioscience Inc.	Cat# 120001400A
Verso cDNA synthesis Kit	Thermo Fischer Scientific	Cat# 1453A
Glucose-6-Phosphate Dehydrogenase Assay kit	Cayman Chemicals	Cat# 700300
Experimental Models: Cell Lines		
Human: Capan-1	American Type Culture Collection	Cat# ATCC HTB-79
Human: PANC-1	American Type Culture Collection	Cat# ATCC CRL-1649
Human: CFPAC-1	American Type Culture Collection	Cat# ATCC CRL-1918
Human: BxPC-3	American Type Culture Collection	Cat# ATCC CRL-1687

(*Continued on next page*)

Continued

REAGENT	SOURCE	IDENTIFIER
Human: HPAF-II	American Type Culture Collection	Cat# ATCC CRL-1997
Human: AsPC-1	American Type Culture Collection	Cat# ATCC CRL-1682
Human: SUIT-2	Gift from Dr. Michael Hollingsworth	Authenticated by STR profiling at UAGC
Human: Colo 357	Gift from Dr. Michael Hollingsworth	Authenticated by STR profiling at UAGC
Human: MIA PaCa-2	American Type Culture Collection	Cat# ATCC CRL-1420
Human: S2-013	Gift from Dr. Michael Hollingsworth	Authenticated by STR profiling at UAGC
Human: T3M4	Gift from Dr. Michael Hollingsworth	Authenticated by STR profiling at UAGC
Human: S2-007	Gift from Dr. Michael Hollingsworth	Authenticated by STR profiling at UAGC
Human: Panc 03.27	American Type Culture Collection	Cat# ATCC CRL-2549
Human: Capan-2	American Type Culture Collection	Cat# ATCC HTB-79
Human: HuP-T3	Gift from Dr. Michael Hollingsworth	Authenticated by STR profiling at UAGC
Human: PaTu 8902	Gift from Dr. Michael Hollingsworth	Authenticated by STR profiling at UAGC
Human: QGP-1	Gift from Dr. Michael Hollingsworth	Authenticated by STR profiling at UAGC
Experimental Models: Organisms		
Mouse: Athymic *Foxn1*^{nu}/*Foxn1*^{nu}	Charles River Laboratories	N/A
Oligonucleotides		
Primers for qPCR	Eurofins MWG operons	(See Table S3)
Primers for ChIP		
ChIP-h*CTPS1* (-744)-F	Eurofins MWG operons	TCCTGAGTAGCTGGGACTACA
ChIP-h*CTPS1* (-744)-R	Eurofins MWG operons	TCACAAGGTCAGGAGTTCAAGA
ChIP-h*CTPS1* (-143)-F	Eurofins MWG operons	AGCAAGCACCCATAACAACC
ChIP-h*CTPS1* (-143)-R	Eurofins MWG operons	GCTGCTTTGGATGGACTAGG
ChIP-h*TKT* (-800)-F	Eurofins MWG operons	CAAGACCTGCCTGGGTAAAG
ChIP-h*TKT* (-800)-R	Eurofins MWG operons	GAGTGATTACAGCTGCCTGAAG
Recombinant DNA		
pRSG1-U6-sgXX-CMV-Cas9	CELLECTA	N/A
sgRNA-hHIF1A target sequence #1	Eurofins MWG operons	AGGATGCTTGCCAAAAGAGG
sgRNA-hHIF1A target sequence #2	Eurofins MWG operons	CAGACACCTAGTCCTTCCGA
Software and Algorithms		
Metaboanalyst 3.0		www.metaboanalyst.ca
MassLynx 4.1	Waters Inc.	www.waters.com/waters/en_US/MassLynx
MVAPACK	Worley and Powers, 2014	http://bionmr.unl.edu/mvapack.php
Chenomx NMR Suite 7.6	Chenomx Inc.	www.chenomx.com/
NMRViewJ	One Moon Scientific	www.onemoonscientific.com/nmrviewj
NMRPipe	NIH, Bethesda, Maryland	https://spin.niddk.nih.gov/bax/NMRPipe/

CONTACT FOR REAGENT AND RESOURCE SHARING

Further information and request for resources and reagents should be directed to the lead contact: Pankaj K. Singh (pankaj.singh@unmc.edu).

EXPERIMENTAL MODEL AND SUBJECT DETAILS

Cell Lines

Capan-1 (source: male), Capan-2 (source: male), PANC-1 (source: male), CFPAC-1 (source: male), BxPC-3 (source: female), HPAF-II (source: male), AsPC-1 (source: female), SUIT-2 (source: male), FG/Colo 357 (source: female) and MIA PaCa-2 (source: male) pancreatic cancer cells were obtained from the American Type Culture Collection (Rockville, MD). S2-013 and S2-007 are cloned sub-lines of a human pancreatic tumor cell line (SUIT-2; source: male) derived from a liver metastasis. S2-013, S2-007, SUIT-2, Panc 03.27 (source: female), HuP-T3 (source: male), QGP-1 (source: male), PaTu 8902 (source: male), and T3M4 (source: male) cell lines were a generous gift from Dr. Michael Hollingsworth (Eppley Institute, UNMC, Omaha, NE). All the cell lines were cultured

in Dulbecco's Modified Eagle Medium (DMEM) supplemented with 10% fetal bovine serum, penicillin (100 mg/ml) and streptomycin (100 mg/ml), and incubated at 37°C in a humidified chamber with 5% CO_2. All cells were passaged with 0.25% trypsin/2.21 mM EDTA in PBS when they reached a confluency of 75-80%. The cell lines were validated by STR profiling at University of Arizona Genetics Core (UAGC).

In Vivo Mouse Studies

Female athymic nude mice (*Foxn1*^{nu}/*Foxn1*^{nu}) age 4-6 weeks were purchased from Charles River Laboratories and housed in the Animal Facility at the University of Nebraska Medical Centre, Omaha, USA. All procedures were approved by the University of Nebraska Medical Centre Institutional Animal Care and Use Committee and in accordance to NIH guidelines. For all the treatment studies mice were randomly assigned to different treatment group. For xenograft studies, after establishing tumor mice were randomly distributed in different group.

Human Studies

The age, tumor grade, and sex of the subjects is provided in Table S1. Sample size information is indicated in the figure legends. All the studies with human subjects were approved by the UNMC IRB committee the committee. Also, informed consent waiver was approved by the UNMC IRB committee for all subjects.

METHOD DETAILS

Glucose Uptake Assay

WT and Gem-R cells were treated with the indicated agents for 12 hr and glucose uptake was performed by utilizing [^{3}H]-2-DG as previously described (Shukla et al., 2014).Briefly, 5X10^4 cells were seeded per well in 24 well plate and incubated over-night at 37°C with 5% CO_2. Next day, cell were starved for glucose for 2 hr and then treated with 1 μCi [^{3}H]-2-deoxyglucose (DG) for 20 min. After incubation, cells were washed twice with PBS and lysed in 1% SDS. Lysates were transferred to scintillation vials containing scintillation fluid. The vials were subjected to [^{3}H] counting by utilizing automated scintillation counter. The values were normalized with respective cell counts.

Mass Spectrometric Metabolomics Analysis

Cells were seeded in 6 cm plates and two hours before the collection of metabolites the culture medium was replaced with fresh medium. Polar metabolites were extracted and then analyzed with LC-MS/MS using the selected reaction monitoring (SRM) method with positive/negative ion polarity switching on a Xevo TQ-S mass spectrometer (Gunda et al., 2016; Yuan et al., 2012). Peak areas integrated using MassLynx 4.1 (Waters Inc.) were normalized to the respective protein concentrations and the resultant peak areas were subjected to relative quantification analyses by utilizing Metaboanalyst 3.0 (www.metaboanalyst.ca) (Xia and Wishart, 2016).

Lentiviral Knockdown/Knockout

shRNA-mediated knockdown of *HIF1A* and *HIF2A* in WT and Gem-R (Capan-1 and T3M4), and GLS and GLS2 in T3M4 Gem-R cells were generated using targeted sequences described previously (Chaika et al., 2012a; Cheng et al., 2011). Single vectors carrying Cas9 nuclease and CRISPR sgRNA targeting control or different regions of *HIF1A* were utilized to establish *HIF1A* knockout. CRISPR sgRNA-Cas9 cassettes were lentivirally transduced to WT and Gem-R cells. Cells were selected against puromycin.

FACS Sorting for GLUT1-High and -Low Cells

2.5x10^6 Capan-1 Gem-R cells plated in a 10 cm dish were gently trypsinized and washed in cold PBS with 1% BSA twice. Cells were incubated with primary antibody for GLUT1 (Abcam, 1:200) for 45 min on ice. The cells were then washed thrice with cold PBS containing 1% BSA, and incubated with Alexa-488-conjugated secondary Ab for 30 min. The cells were finally washed thrice and sorted by flow cytometry for high- and low-GLUT1 expression.

MTT Cytotoxicity Assays

A total of 6,000 cells/well were plated in 96 well plates 12 hr before the treatment. The cells were then treated with indicated agents for 72 hr. At the end of the treatment, 10% v/v of 5-mg/ml solution of 3-[4,5-dimethylthiazol-2-yl]-2,5-diphenyltetrazolium bromide (MTT) agent was added for 2 hr. The medium was then removed and the cells were dissolved in DMSO (Sigma, St Louis, MO). Relative cytotoxicity was determined by measuring the absorbance at 570 nm using a BMG Labtek plate reader. All experiments were done in triplicates and a mean with SEM was calculated.

Clonogenic Assays

Capan-1 and T3M4, WT and Gem-R cells were treated with gemcitabine (concentrations indicated) for 72 hr, followed by plating 500 cells per well in 6 well plates. Colonies were stained and imaged 18 days later using 0.2% crystal violet in 80% methanol.

Soft Agar Assays

5000 cells were suspended in 1 ml top agar made of 0.4% NuSieve GTG agarose in DMEM and seeded over 2 ml of bottom agar composed of 0.8% NuSieve GTG agarose in DMEM. Colonies were counted after 15 days and colony size measured by pictomicrography.

Glutamine Uptake Assay

Pancreatic cancer cells were seeded in 24 well plates. At the end of the treatment, the control wells were treated with 4 mM of glutamine for 10 min, followed by addition of 4 μl of [^{3}H]-glutamine (Perkin Elmer). The cells were washed and lysed in 1% SDS followed by measurement of radiolabel using a scintillation counter. The raw values were normalized to cell counts.

XF24 Extracellular Flux Analysis

Extracellular acidification rate (ECAR) and oxygen consumption rate (OCR) analyses were performed with an XF24 extracellular flux analyzer (Seahorse Biosciences, North Billerica, MA) as described previously (Wu et al., 2007). Briefly, 3.5x10^4 cells were seeded per well in 24-well cell culture plates (Seahorse Biosciences, North Billerica, MA) in DMEM with 10% FBS and incubated at 37°C, overnight in 5% CO_2 incubator. Next day, growth medium was replaced with bi-carbonate free DMEM and cells were incubated at 37°C for 1 hr in CO_2 free incubator to equilibrate media temperature and pH. By utilizing a Seahorse XF24 analyzer, ECAR and OCR were measured in baseline conditions and under treatment with 2,4-dinitrophenol (2,4 DNP; 100 μM), 2-deoxy glucose (2-DG; 100 mM) and rotenone (1 μM). Values ae presented as mean ± standard error of mean.

1-^{14}C- and 6-^{14}C-Glucose CO_2 Release Assay

CO_2 release assay was performed as previously described (Ying et al., 2012). Briefly, cells were treated with 1 μCi of 1-^{14}C- and 6-^{14}C-glucose followed by incubation at 37°C for the indicated durations. At the end, 150 μl of 3M perchloric acid was added and the wells were immediately covered with Whatmann's filterpaper dipped in phenylethylamine. The released radiolabeled CO_2 captured on the filter paper was measured with a scintillation counter.

Lactate Release Assay

Lactate levels secreted into the media were analyzed by colorimetric assays. The assay was performed as per the manufacturer's protocol utilizing Lactate Assay Kit II (Eton Bioscience Inc.).

Glucose-6-Phosphate Dehydrogenase Assay

Glucose 6-phosphate dehydrogenase activity was measured by flurometric measurement. The assay was performed as per manufacturer's protocol by utilizing Glucose-6-Phosphate Dehydrogenase Assay Kit (Cayman Chemicals).

Gene Expression Analysis by Real-Time PCR (qPCR)

Total RNA was isolated by using RNAeasy columns (Quiagen) as per manufactures protocol. Total RNA (5 μg) was reverse transcribed by using Verso-cDNA synthesis kit (Thermo-Scientific) according to the manufacturer's guidelines. qPCR was performed with gene specific primers at 95°C for 10 sec, 60°C for 60 sec (40 cycles) in 10μl reaction mix containing 3μl cDNA, 2 μl primers and 5 μl SYBR Green master mix (Applied Biosystems) using an ABI 7900 thermocycler. Beta-actin was used as an internal control. Quantification was performed with the ΔΔCt method (Schmittgen and Livak, 2008). See Table S3 for the primer sequences used for qPCR analysis. All the mRNA correlations with gemcitabine IC_{50} were performed by utilizing the following cell lines: Capan-1, PANC-1, CFPAC-1, BxPC-3, HPAF-II, AsPC-1, SUIT-2, Colo 357, MIA PaCa-2, S2-013, T3M4, S2-007, Panc 03.27, Capan-2, HuP-T3, PaTu 8902, and QGP-1.

Chromatin Immunoprecipitation Analysis

ChIP assays were performed as described previously (Behrens et al., 2010). 3.0 μl purified chromatin for ChIP analysis were used with Sybr green master mix (Applied Biosystems, Foster City, CA, USA) and subjected to qPCR analysis using ABI 7900 thermocycler. Each reaction was performed in triplicate and the experiments were repeated at least twice to confirm reproducibility. Values were obtained for the threshold cycle (Ct) for each gene or genomic region and data were analyzed using the standard curve method. For ChIP qPCR analysis, values were normalized to an input control and expressed as a fold increase over enrichment detected using IgG, as published previously (Behrens et al., 2010). The average expression ± S.E.M. was reported. See the Key Resources Table for primer sequences.

Immunoblotting

Cell lysates were prepared by scraping cells (225 cm^2, 80-90% confluent) into 1.5 mL of lysis buffer (50 mM Tris-HCl pH 8.0 containing 1% NP-40, 150 mM NaCl, 5 mM EDTA and 1 mM phenylmethylsulphonyl fluoride). Western blottings were performed as previously described (Singh et al., 2008). The membranes were probed with primary antibodies against HIF1α (BD Biosciences), MUC1 (Abcam), GLUT1 (Abcam) and LDHA (Abcam).

Immunohistochemistry

Immunohistochemistry was performed by utilizing goat anti-rabbit IgG-AP with Fast-Red to produce red stain (PicTure™-Double Staining kit, Invitrogen), as per the manufacturer's instructions. Following primary antibodies were utilized: Ki67 (Thermo Fisher), CTPS (Sigma) and TKT (Sigma). The stained sections were imaged at 200 X under an inverted microscope. Cells with Ki67 positive nuclear staining were counted in 3 random fields at 200 X magnification. The intensity score was given by evaluating staining intensity of positive staining (0 = none; 1 = weak; 2 = intermediate, 3 = strong). The proportion score representing the percentage of positively stained cell (0 = none; 1 = less than 5%; 2 = 5–25%; 3 = 26–50% 4 = 51–75% 5 = above 75%). The overall protein expression in each sample is expressed as histoscore, which is the multiplication product of the proportion (0–5) and intensity scores (0–3) and is between 0–15, with a maximum of 15. The staining score was evaluated by two independent pathologist-trained observers.

Hypoxia Imaging and Co- localization with CTPS and TKT

Hypoxia imaging in tumor tissues and co-localization of CTPS or TKT with EF5 or CA IX by immunofluorescence microscopy was performed as described previously (Chaika et al., 2012a). Briefly, tumor-bearing mice were injected with100 micro liter EF5 solution (3 mg/ml) three hours before necropsy. After necropsy tumor pieces were flash-frozen. Seven micrometer thick Flash-frozen tumor sections were then first stained with anti-CTPS/ anti-TKT antibodies followed by staining with Cy3-conjugated anti-EF5 monoclonal antibody along with Alexa-488 anti-Rabbit polyclonal antibodies. Tissue sections were stained with mouse anti-CA IX antibody along with rabbit anti-CTPS or anti-TKT antibodies where applicable. Sections were counterstained with DAPI. Immunofluorescence images were captured by using Leica DMI6000B microscope at 200 X magnification.

Tumor Growth Studies

Congenitally athymic female nude mice (NCr-nu/nu) were purchased from the Charles River Laboratories, USA. We orthotopically implanted $0.5x10^6$ WT or Gem-R cells in the pancreas of athymic nude mice. Starting day 7 post-implantation, the mice were treated with digoxin (2 mg/kg, daily), leflunomide (10 mg/kg/day), gemcitabine (50 mg/kg, biweekly), YC1 (15 mg/kg, daily), PBS (100 μl, daily), saline control or combinations. Mice were monitored for a period of 30 days and were sacrificed when the tumor reached 1000 mm^3 in dimension. For the macroscopic evaluation of metastasis, we considered occurrence of metastasis if at least one metastatic nodule was present in an organ.

Patient-Derived Xenograft (PDX) Studies

Six to eight-week-old female athymic nude mice were used to implant PDX tumors. Tumor samples were cut in to 3-4 mm pieces and immediately placed in F-12 HAM (SIGMA-ALDRICH, MO, USA) medium supplemented with 50% fetal calf serum and 50 units/ml penicillin and 50 microgram/ml streptomycin. Tumor tissue pieces were embedded into Matrigel before subcutaneous implantation into mice. After implantation of tumor tissue, xenografts were allowed to grow for 4 weeks. When tumor size reached 150 mm^3, mice were divided into four groups (vehicle control, gemcitabine (50 mg/kg, twice per week), digoxin (2 mg/kg, per day) and digoxin with gemcitabine), and treated for 18 days. Tumor volume and body weight were recorded regularly during the treatment. After 18 days of treatment mice were sacrificed and tumor volume, tumor weight etc. were measured. Patient-derived xenograft PATX162 was implanted in nude mice with previously published method (Kim et al., 2009) at MD Anderson Cancer Center. Briefly, tumor pieces were divided in 4-5 mm pieces and placed into Matrigel. Matrigel-embedded tumor pieces were then subcutaneously implanted to both flanks of athymic nude mice. Six to eight-week-old athymic female nude mice were utilized for subcutaneous implantation. When tumors reach the size of ~100 mm3 mice divided into 4 groups with 5 mice in each group. Mice were treated for 6 weeks with gemcitabine at 50 mg/kg twice a week, digoxin at 2 mg/kg daily, through intraperitoneal injection, or the combination of both agents. The mice were sacrificed when their tumors reached the size of 15 mm in diameter.

In Vivo Glucose Uptake Assays

Three female athymic *Foxn1^{nu}/Foxn1^{nu}* mice per group were intraperitonially injected with 10 nmoles of the XenoLight RediJect-2DG 750 optical probe (Perkin Elmer Inc.) in 100 μl PBS per mouse (as per the manufacturer's recommendations). Animals were then imaged using IVIS Spectrum small animal imaging system.

NMR Metabolite Extraction

Cells were harvested at 70-80% confluence. After removing the media by aspiration and washing twice with 1X PBS to remove remnants of the media, metabolites were extracted with 1 ml of cryogenically cold 80% methanol. The plates were then incubated at −80°C for at least 15 min. Scrapers were used to scrap the cells from the plate and transferred in to an Eppendorf tube. The tube centrifuged at 13,000 rpm for 5 min to separate the cell extract from the cell debris. The supernatant was then transferred to a clean tube and 250 μl of Milli-Q water (Millipore, Billerica, MA, USA) was added to the remaining cell debris for re-extraction. The cell debris were mixed with the water by pipetting. The samples were centrifuged to collect the aqueous extract and the collected water extract was mixed with the 80% methanol extract. Vacuum evaporator (SpeedVac® Plus, Savant, Thermo Scientific, Waltham, MA) and lyophilizer (Labconco, Kansas City, MO) were utilized to evaporate the methanol and lyophilize the water, respectively. The dried samples were dissolved in 600 μl of 50 mM phosphate buffer in 99.8% D2O (Isotec, St. Louis, MO) at pH 7.2 (uncorrected) with 50 μM 3-(tetramethysilane) propionic acid-2,2,3,3-d4 (TMSP) for spectral referencing. The solution was centrifuged down at 13000 for 5 min and the supernatant was transferred to 5 mm NMR tube.

NMR Experiment

Bruker AVANCE DRX 500 MHz spectrometer equipped with 5 mm triple-resonance cryogenic probe (1H, 13C and 15 N) with a Z-axis gradient was utilized to acquire the NMR data. The experiment was automated using BACS-120 sample changer, ATM (automatic tuning and matching) and Bruker IconNMR™ software. The one-dimensional (1D) proton nuclear magnetic resonance (1H NMR) data were collected at 300 K with 32 K data points, 128 scans, 16 dummy scans and a spectral width of 5,483 Hz using an excitation sculpting pulse sequence (Nguyen et al., 2007). The 2D ^{1}H-^{13}C hetero-nuclear single quantum coherence (HSQC) NMR spectra were collected with 2 K data points and a spectrum width of 4,735 Hz in the direct dimension and 64 data points and a spectrum width of 17,607 Hz in the indirect dimension at 300 K with 64 scans, 16 dummy scans and a 1.5 s relaxation delay.

NMR Data Analysis

The 1D-^{1}H NMR data were analyzed using MVAPACK software (http://bionmr.unl.edu/mvapack.php) (Worley and Powers, 2014). The raw NMR data was Fourier transformed, automatically phased and binned using adaptive intelligent binning (De Meyer et al., 2008). The spectra were then normalized using standard normal variate (SNV) and the noise was removed. This data was used to generate principal component analysis (PCA) model. The intact spectrum was normalized using SNV, noised was removed and scaled using Pareto scaling to generate orthogonal projections to latent structures discriminant analysis (OPLS-DA) scores and back-scaled loadings. Metabolite identification from the 1D 1H NMR spectra and backscaled loading were accomplished using the Chenomx NMR Suite 7.6 (http://www.chenomx.com/). NMRPipe (NIH, Bethesda, Maryland) and NMRViewJ Version 8.0.3 were used to process and analyze the 2D 1H-13C HSQC NMR spectra respectively. 2D-^{1}H-13C HSQC NMR spectra peak intensities were normalized by the average peak intensity for a given spectrum. The Human Metabolomics Database (Wishart et al., 2013), Madison Metabolomics Consortium Database (Cui et al., 2008) and Platform for RIKEN Metabolomics (Akiyama et al., 2008) were used for peak assignment.

[^{18}F]FDG-PET, Magnetic Resonance Imaging

[^{18}F]FDG-PET imaging was performed as described previously (Schlaepfer et al., 2015). We performed single-position, whole-body imaging by using a Siemens Inveon microPET scanner at the University of Colorado Cancer Center Animal Imaging Shared Resources (AISR). Mice were fasted for 6 h before [^{18}F]FDG injection, and blood glucose levels was assessed prior to the [18F]FDG injection (all animals had < 80 mg/ml of circulating glucose). Approximately 250 μCi of [^{18}F]FDG, obtained through University of Colorado Hospital (PetNet solutions), was administered by tail vein injection to conscious animals (the precise dose was assessed by measuring the syringe before and after the injection) (Morelli et al., 2012). Animals were maintained in temperature-controlled cages for 1 h to allow for awake [^{18}F]FDG uptake in tumors. Under isoflurane anesthesia (2.5 %), animals were placed on a warm pad (m2m Imaging), and a 10 min emission scan was acquired. [^{18}F]FDG uptake in mouse orthototpic tumors, as well as control tissues (muscle) was performed by analyzing the micro-PET images with the ASIProVM (Concorde Microsystems) software. Regions of interest were drawn with the trace command around the tumors on scan slices, and the total activity of all tumor slices was summed. The normalized uptake values (NUVs) were obtained by dividing the total activity of the tumor by the time-corrected dose-delivered [time-corrected dose = dose injected x exp(−0.006317 x t)], where t is the time between the injection and scan time, and it is shown as the fold change of the baseline scan of each respective tumor. Representative images were generated using the Siemens Inveon Research Workplace software (v3.1.2).

Detection of Gemcitabine and dCTP

Relative quantification of Gemcitabine in the cell lysates was performed using LC-MS/MS-based method. Dried cell extracts were reconstituted in mass spec grade water followed by chromatography through Synergi Hydro-Reverse Phase column (150x2.0 mm, Phenomenex) maintained at room temperature. The chromatography method included a gradient with increase of Buffer B (100% methanol) linearly with simultaneous decrease in the content of Buffer A (20 mM Ammonium acetate, pH 5.0) till 10 min and returning to initial concentration at 12 min. Gemcitabine elution and detection were performed using Waters Acquity UPLC coupled to Xevo TQ-S mass spectrometer. For detecting dCTP dried cell extracts were reconstituted in mass spec grade water followed by chromatography using HSS-T3 column (100X2.0 mm, Waters). Chromatography method constituted a linear gradient with increase of Buffer A (10 mM Ammonium formate, pH 6.5) from 0 to 50% in 5 min, hold at 50% for 3 min, followed by a decrease to 0% by 13 min and final rinse of column at 100% B (100% Acetonitrile) till 15 min. The dCXP correlations with gemcitabine IC_{50} (Figure 4E) were performed by utilizing the following cell lines: Capan-1, PANC-1, CFPAC-1, BxPC-3, HPAF-II, SUIT-2, Colo 357, MIA PaCa-2, S2-013, T3M4, S2-007, Panc 03.27, Capan-2, HuP-T3, and PaTu 8902.

LC-MS/MS for Polar Metabolites and ^{13}C-Glucose Based Flux Analysis

Relative quantification of polar metabolites including deoxycytidine and ^{13}C-labeled metabolites was performed using selected reaction monitoring and scheduled reaction monitoring based mass spectrometry methods, respectively. Liquid chromatography method used for separating unlabeled and labeled metabolites constituted an UPLC-based BEH amide column (150x2.1 mm, Waters) eluted with a gradient buffer composition consisting of Buffer A (100% Acetonitrile) and Buffer B (20 mM Ammonium acetate, pH 9.0) (Gunda et al., 2016).

QUANTIFICATION AND STATISTICAL ANALYSIS

Nonparametric one-way ANOVA (Kruskal-Wallis tests) were utilized to compare differences between animal groups. One-way ANOVA with Dunnett's test was performed to determine the effect of inhibitors on treated and Gem-R cells, as compared to the WT cells. One-way ANOVA alone was performed to determine the effect of different inhibitors on one cell type (WT or Gem-R). Patient survival data was compared by Kaplan Meier survival analysis using Log-rank (Mantel-Cox) test. Student's t-test was used when appropriate. $P < 0.05$ was considered significant. All statistical tests were performed by utilizing GraphPad Prism5 and SPSS 16.0 software. For all experiments * $p < 0.05$, ** $p < 0.01$, and *** $p < 0.001$.